University of Alberta

Morphological Studies of Polyethylene

by

Mingtao Wang ©

A thesis submitted to the Faculty of Graduate Studies and Research in
partial fulfillment of the requirements for the degree of Master of Science

in

Chemical Engineering

Department of Chemical and Materials Engineering

Edmonton, Alberta

Spring, 2006

Canada

Abstract

The structure of polyethylene has been investigated for decades; however, our understanding, especially for linear low-density polyethylene (LLDPE), is still incomplete. This greatly impedes progress in establishing structure-property relationships. In this thesis, solid-state NMR spectroscopy, gel permeation chromatography (GPC), fuming nitric acid (FNA) etching, and differential scanning calorimetry (DSC), have been utilized to explore the morphological features of polyethylenes. It was found that single-site (ss-) and Ziegler-Natta (ZN-) LLDPEs contain three distinct phases, namely, the crystalline, crystalline-amorphous interfacial, and amorphous components; under similar crystallization conditions, ZN-LLDPE has a higher degree of crystallinity and a lower mass fraction of the interphase than ss-LLDPE. The results also show that ZN-LLDPE has a greater average lamellar thickness and a broader lamellar thickness distribution compared to those of ss-LLDPE. The average thickness of the interfacial zone for ss-LLDPE was found to be 3.9 nm, while that for ZN-LLDPE was 2.6 nm.

The partitioning of branches between the interfacial and amorphous regions is also an important structural feature. The ^{13}C spin-spin (T_2) relaxation process for the CH_2 carbons within the non-crystalline regions and CH carbons at the branching sites of two types of LLDPEs was investigated. The results show that the hexyl branches are not very uniformly distributed between the interfacial and amorphous regions. For ss-LLDPE, the interfacial region has a greater density of branches. For ZN-LLDPE, the amorphous region has a greater density of branches.

Acknowledgements

I would like to take this opportunity to express my sincere gratitude to my supervisors Drs. Phillip Choi and Roderick E. Wasylishen for their unfailing encouragement, and insightful guidance for both my research work and daily life.

I also would like to thank my wife, Wei Sun, whose confidence in me never wavers, for her love and support during and beyond the period of my study at the University of Alberta.

Sincere gratitude also goes to my parents, Wenjin Wang and Cuifang Wang, and to my sister, Xiufeng Wang, who always understand and support me without any reservation.

I would like to thank the members from both the polymer and solid-state NMR groups for their help during my study. Especially, I would like to thank Dr. Guy M. Bernard for his tremendous help with the solid-state NMR experiments.

Table of Contents

LIST OF TABLES

LIST OF FIGURES

Nomenclature

B_0 static magnetic field of an NMR spectrometer

B_1, B_2 r.f. magnetic fields associated with v_1, v_2

M_x x-component of macroscopic magnetization

M_y y-component of macroscopic magnetization

M_z z-component of macroscopic magnetization

M_0 equilibrium macroscopic magnetization of a spin system in the presence of B_0

T temperature

T_1 spin-lattice relaxation time

T_2 spin-spin relaxation time

$T_{1\rho}$ spin-lattice relaxation time in the rotating frame

v_1 frequency of observing r.f. magnetic field

v_2 frequency of irradiating r.f. magnetic field

τ time between r.f. pulses

T_d pulse delay

$S(t)$ intensity of the peak at time t

$S(\infty)$ intensity of the peak at time $t > 5T_1$

M_n number-average molecular weight

M_w weight-average molecular weight

M_z z-average molecular weight

t_e etching time

L_n number-average length

L_w weight-average length

δ chemical shift

Abbreviations

CPMG	Carr-Purcell pulse sequence, Meibon-Gill modification
CW	continuous wave
DD	dipole-dipole (interaction or relaxation mechanism)
FID	free induction decay
FT	fourier transform
NMR	nuclear magnetic resonance
ppm	parts per million
r.f.	radio frequency
S/N	signal-to-noise ratio
TMS	tetramethylsilane
mol. wt.	molecular weight
GPC	gel permeation chromatography
FNA	fuming nitric acid
PE	polyethylene
HDPE	high-density polyethylene
LDPE	low-density polyethylene
LLDPE	linear low-density polyethylene
o.d.	outside diameter
PDI	polydispersity
TTPM	two-pulse phase modulation

CHAPTER 1

Introduction

1.1 Polyethylene (PE)

Polyethylene is the world's highest volume plastic owing to its excellent processability, light weight, low cost and safety. Polyethylene has found a variety of applications such as packaging, consumer goods, pipes, durable equipment, and industrial machinery. Every year, over 60 million tons of polyethylene are produced worldwide [Wikipedia contributors 2005]. The demand will continue to increase over the next five years.

Polyethylene includes a broad range of homo- and co-polymers for which ethylene is the main building unit. Various types of polyethylenes are commercially available. The first type of polyethylene that was commercially available is low-density polyethylene (LDPE), which was discovered by Fawcett and Gibson at ICI in England in the early 1930's. LDPE is characterized by having a highly branched structure and has its main application in films [Seymour and Cheng 1986, 1987]. High-density polyethylene (HDPE) became commercially available with the discovery of catalysts that permit the synthesis of linear chains that contain very little or no branches [Seymour and Cheng 1986, 1987]. HDPE is mostly used in molded containers and pipes [Lohse 2000]. The third type of polyethylene is linear low-density polyethylene (LLDPE), which can be produced by Ziegler-Natta and single-site catalysts in a variety of molecular architectures with differing processing

and α-olefins. The most commonly used α-olefins are 1-butene, 1-hexene and 1-octene [Young and Lovell 1991]. In contrast, both HDPE and LDPE are homo-polymers produced by polymerizing ethylene monomers. LLDPE is mainly used for film applications [Seymour and Cheng 1986, 1987; Lohse 2000]. The molecular structures of these three polyethylenes are shown in Figure 1.1.

High-density polyethylene

Low-density polyethylene

Linear low-density polyethylene
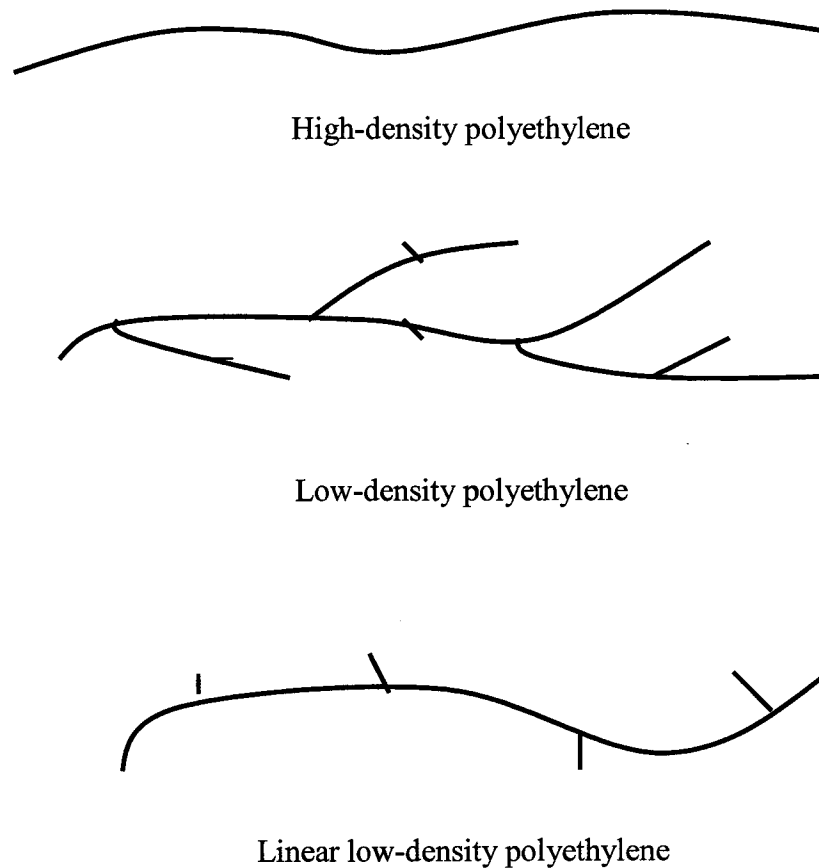
Figure 1.1 Molecular structures of different polyethylenes.

Polyethylene is one of the most analyzed polymers, due to its great importance in both scientific and industrial communities; yet, a complete understanding of the relationship between polyethylene structure and its mechanical performances is still lacking. Therefore, study of structure-property correlation of polyethylene is still an active research area. Construction of a complete structure-property correlation is beyond the scope of this thesis. However, an important step, namely, the elucidation of the morphological features of polyethylenes, was fulfilled and is presented in this thesis. Tensile tests on selected polyethylene films are also included.

1.2 Objectives of this Thesis

The main objective of this thesis is to elucidate the structural characteristics of polyethylenes. In particular, the detailed morphologies of Ziegler-Natta (ZN-) and single-site (ss-) LLDPEs are investigated. Evaluation of the tensile strengths of selected polyethylene films has also been performed.

1.3 Structure of this Thesis

This thesis consists of seven chapters. Chapter 2 presents a review and discussion of the literature that is pertinent to this project.

In Chapter 3, the principal experimental tool, solid-state nuclear magnetic resonance (NMR) spectroscopy, is introduced. In particular, solid-state ^{13}C NMR techniques that are used for the structural elucidation of polymers are discussed in detail.

Solid-state ^{13}C NMR techniques, combined with fuming nitric acid (FNA) etching and gel permeation chromatogram (GPC), were utilized to investigate the morphological features of ss- and ZN-LLDPE bulk samples. Chapter 4 describes this methodology and the results obtained thereby.

Chapter 5 describes the determination of the phase structure of HDPE blown films, and the clarification of the location of the short-chain branches for two types of LLDPEs, by using solid-state ^{13}C NMR techniques.

Tensile tests on selected polyethylene films are discussed in Chapter 6.

Major findings of this study and recommendations for future work are discussed in Chapter 7.

1.4 References

Lohse, D. J.(2000) The chapter "Polyolefins" in the book of " Applied Polymer Science: 21st Centaury", edited by Craver, C. D. and Carraher Jr., C. E., and published by Elsevier Science Ltd, Oxford, UK.

Seymour, R. B. and Cheng T. (1986) History of Polyolefins, D. Reidel Publishing Company, Dordrecht, Holland.

Seymour, R. B. and Cheng T. (1987) Advances in Polyolefins: the World's Most Widely Used Polymers, Plenum Press, New York, USA.

Wikipedia contributors. (2005) "Polyethylene," *Wikipedia, The Free Encyclopedia,* http://en.wikipedia.org/w/index.php?title=Polyethylene&oldid=31629721.

Young, R.J. and Lovell P.A. (1991) Introduction to Polymers (Second Edition), Nelson Thornes Ltd, UK.

CHAPTER 2

Literature Review

2.1 Morphological Studies of Polyethylene

Polyethylene is the most studied polymer because of its many applications. The mechanical properties of polyethylene products are dictated by their structures; therefore, an understanding of the relationship between structure and property is vital to improving the performances of the materials. Structural elucidation is the most important step towards constructing structure-property relationships. Such relationships are not only important to academics but have significant value to the polymer industry.

Morphological studies of polyethylene are discussed from the following aspects: the phase structure, the degree of crystallinity and crystalline lamella size, the thickness of the interfacial region, and the distribution of the short-chain branches. Various experimental techniques, such as solid-state nuclear magnetic resonance (NMR) spectroscopy, gel permeation chromatography (GPC), transmission electron microscopy (TEM), small-angle neutron scattering (SANS), small-angle X-ray scattering (SAXS), etc., have been employed to study the morphological features of polyethylene samples.

Reproduced with permission of the copyright owner. Further reproduction prohibited without permission.

2.1.1 The Phase Structure

The long chain nature of polymers distinguishes them from other materials, because each polymer chain is capable of adjusting its shape in response to both external and internal interactions. Generally, polymer chains experience two quite different environments depending on whether or not they are in ordered (crystalline), or disordered (amorphous) phases. For semi-crystalline polymers, a chain with sufficient structural regularity can spontaneously develop order along a portion of its length and a collection of such chains can then be organized into three-dimensional arrays and form the crystalline lamella. During the crystallization process, those irregular structural units, such as entanglements, knots, loops, etc., will be rejected from the crystalline region, and concentrate in the inter-lamellae regions, known as the amorphous phase. Besides these two regions, researches have long believed that there should be an interfacial region sandwiched between the crystalline and amorphous regions, where the ordered crystalline structure gradually dissipates into a totally disordered amorphous phase [Flory 1962, 1984; Mandelkern *et al.*, 1984, 1990].

Flory [1962] investigated the spatial requirements of polymer chains in the interfacial zone and gave a model of the interfacial zone. As shown in Figure 2.1, this transitional zone (the area between A and B) is transverse to the chain axis. A later review by Mandelkern [1990] addressed the experimental and theoretical developments that have given strong indications of the existence of the interfacial region. Experimental studies, such as ^{1}H and ^{13}C NMR spectroscopy [Kitamaru *et al.* 1977, 1986; Axelson and Russell 1985; Kazuhiro *et al.* 1997], small-angle

neutron scattering [Russell *et al.* 1988], specific heat measurements [Suzaki *et al.* 1985], dielectric relaxation [Hahn *et al.* 1985], and analysis of the Raman internal modes [Strobl and Hagedorn 1978], clearly demonstrate the presence of an appreciable amount of interfacial component which is characterized by the partial ordering of the chains.
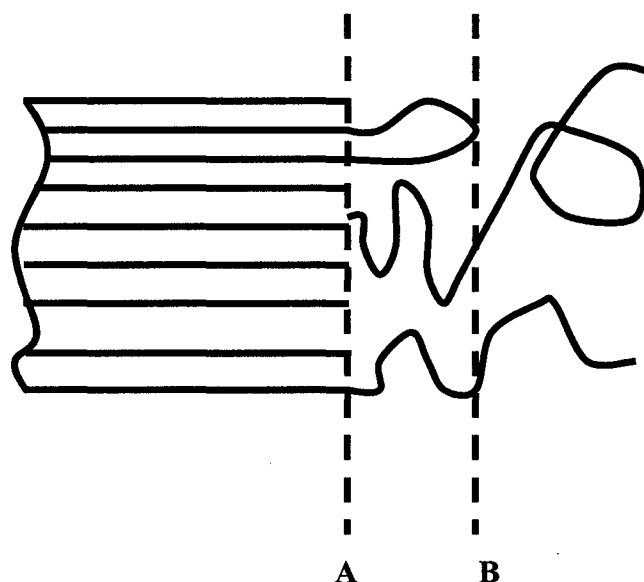
Figure 2.1 Schematic representation of the interfacial zone transverse to the chain axis (after Flory, *J. Am. Chem. Soc.* 1962 (84), 2857).

Kitamaru *et al.* [1986] studied the phase structure of polyethylene samples by high-resolution solid-state ^{13}C NMR spectroscopy. They studied the ^{13}C spin-lattice (T_1) and spin-spin (T_2) relaxation times, and found that HDPE samples crystallized from the melt consist of three phases, namely, the crystalline, crystalline-amorphous interfacial, and isotropic amorphous phases.

- 7 -

Kuwabara *et al.* [1997] studied the crystalline-noncrystalline structure for metallocene-catalyzed linear low-density polyethylene (LLDPE) by solid-state ^{13}C NMR techniques. They found three components with different ^{13}C T_1 and T_2 relaxation times, which they assigned to the crystalline, amorphous, and interfacial phases.

In a review paper [Horii *et al.* 1998], solid-state NMR techniques which can be utilized to investigate the structure of polyethylene have been discussed. The authors stated that: "High-resolution solid-state ^{13}C NMR is a very powerful method for characterizing such a crystalline-noncrystalline structure, particularly for discriminating between the interfacial and amorphous regions in terms of ^{13}C spin-spin relaxation times T_2 measured without ^{1}H dipolar decoupling." As a result of solid-state ^{13}C NMR analyses, the authors present a morphological model for HDPE, which is shown in Figure 2.2.
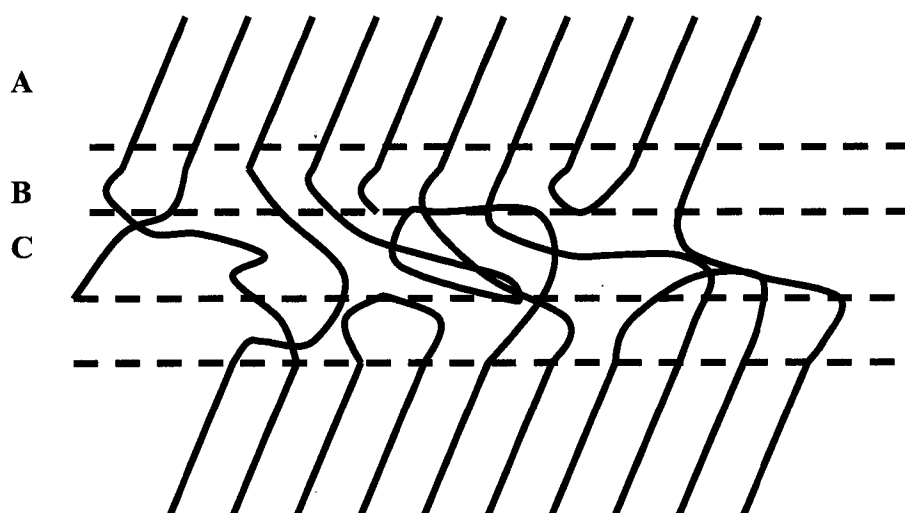
Figure 2.2 A schematic representation of the three phases for HDPE isothermally crystallized from the melt (after Horii *et al.*, *J. Mol. Struc.* 1998 (441), 303).

- 8 -

As demonstrated in Figure 2.2, region A is the crystalline component, B is the interphase, and C is the amorphous component. The interfacial components are situated between the crystalline and amorphous regions, where the chains gradually change from ordered state to totally disordered random coils.

2.1.2 The Crystalline Lamella Length and Its Distribution

The thickness and its distribution of the crystalline lamellae in polymer samples is a factor which is of fundamental importance in determining the physical properties of the polymer. Experimental techniques which have been used to study this quantity are low-frequency Raman longitudinal acoustic mode (LAM) spectroscopy, small-angle X-ray scattering (SAXS), electron microscopy (EM) and fuming nitric acid (FNA) etching followed by GPC measurements. Glotin and Mandelkern [1983] investigated the first-, third-, and fifth-order low-frequency, Raman-active, longitudinal acoustical modes of different polyethylene samples and obtained the crystallite thicknesses through the correlation between the mode and length. Viogt-Martin *et al.* [1989] conducted SAXS, Raman LAM and EM on a number of polyethylene samples and compared the values obtained by these techniques. They found that crystal morphologies and in particular the nature of the thickness distributions are the main factors that cause discrepancies in obtained values. An easy yet powerful method to determine the lamella stem length and its distribution was carried out by Cappaccio and Ward [1981; 1982]. In this method, the crystal size and its distribution can be obtained from the GPC measurements of polyethylene samples which are etched over different time periods.

2.1.3 The Thickness of the Interfacial Zone

Characterization of interfacial structure is an important and difficult problem in polymer science. It is believed that chain re-entry plays an important role in affecting the conformation of the interfacial region [Mandelkern 1990]. Theoretical predictions show that the interfacial thickness for the bulk crystallized HDPE is in the range of 1~3 nm [Kumar and Yoon 1989]. Kuwabara *et al.* [1997] estimated the thickness of the interfacial zone for both metallocene-catalyzed and Ziegler-Natta (ZN-) LLDPE samples based on the information obtained by solid-state ^{13}C NMR spectroscopy and TEM. They showed that the thickness of the interfacial region is about 3 nm for both samples.

2.1.4 The Location of Short-Chain Branches

The partitioning of the short-chain branches among the crystalline, interfacial, and amorphous regions is also an important problem because it affects the crystallization, free volume, and other characteristics of polyethylene samples. It is believed that under equilibrium conditions, methyl branches are readily included into the crystalline region, whereas branches longer than two carbons, such as butyl branches and hexyl branches are excluded from the crystalline region. There are still no definite answers about the partitioning of these longer branches between the interfacial and amorphous regions.

Alamo *et al.* [1984] found that only methyl branches can enter into the lattice under equilibrium conditions based on the investigations of the melting behaviour of various copolymers. Other types of branches, such as ethyl, propyl, butyl, hexyl etc.,

can only enter into the lattice as non-equilibrium defects and invariably cause a lowering of the melting temperature.

VanderHart et al. [1986, 1987] developed a ^{13}C NMR method for determining the partitioning of the ethyl branches between the crystalline and non-crystalline regions. They found that no more than 8% of the ethyl branches resided in the crystalline region under equilibrium conditions.

Kuwabara et al. [1997] employed the method developed by VanderHart et al. [1986, 1987] to determine the partitioning of the butyl branches between the crystalline and non-crystalline regions for metallocene-catalyzed LLDPE isothermally crystallized from the melt. Their results confirmed that all butyl branches are excluded from the crystalline region. They also investigated the partitioning of the branches between the interfacial and amorphous regions by ^{13}C T_2 measurements. By comparing the T_2 relaxation behaviour of the CH carbon at the branching point and the CH$_2$ carbon in the non-crystalline regions, they concluded that the butyl branches are almost equally distributed in the interfacial and amorphous regions.

2.2 Structure-Property Correlation of Polyethylene Films

The morphology of polyethylene films strongly influences their final mechanical properties. Structural parameters, such as density, degree of crystallinity, molecular weight and its distribution, short-chain branching (SCB), and the crystalline morphology, are among the key factors that control the final mechanical properties.

- 11 -

Godshall *et al.* [2003] investigated the processing-structure-property relationships of HDPE blown films and found that the machine and transverse direction oriented lamellar stacks have a substantial influence on the final mechanical properties.

Zhang *et al.* [2004] studied the oriented structure and anisotropy properties of HDPE, LLDPE and LDPE blown films by microscopy and infrared trichroism and found that HDPE, LLDPE, and LDPE films exhibit quite different crystalline morphologies and orientation characteristics. These differences were shown to translate into different ratios of machine and transverse direction tear and tensile strengths.

2.3 References

Axelson, D. E. and Russell, K. E. (1985) Characterization of Polymers by Means of ^{13}C NMR Spectroscopy: (a) Morphology by Solid-State NMR (b) End-Group Studies, *Prog. Polym. Sci.* 11, 221-282.

Alamo, R.; Domszy, R. and Mandelkern, L. (1984) Thermodynamic and Structural Properties of Copolymers of Ethylene, *J. Phys. Chem.* 88, 6587-6595.

Capaccio, G. and Ward, I. M. (1981) Structural Studies of Ultrahigh-Modulus Linear Polyethylene Using Nitric Acid Etching and Gel Permeation Chromatography. I. Determination of the Crystal Size Distribution, *J. Polym. Sci., Polym. Phys. Ed.* 19, 667-675.

Capaccio, G. and Ward, I. M. (1982) Structural Studies of Ultrahigh-Modulus Linear Polyethylene Using Nitric Acid Etching and Gel Permeation

Chromatography. II. Influence of Polymer Molecular Weight, Draw Temperature, and Annealing, *J. Polym. Sci., Polym. Phys. Ed.* 20, 1107-1128.

Earl, W. L. and VanderHart, D. L. (1979) Observations in Solid Polyethylenes by Carbon-13 Nuclear Magnetic Resonance with Magic Angle Sample Spinning, *Macromolecules* 12, 762-767.

Egorov, E. A.; Tshmel, A. E. and Zhizhenkov, V. V. (1998) Structure of the Tie Chains in Orientated Polyethylene: Dependence of All-Trans Stem Lengths on Draw Ratio, *Polymer*, 39, 497-499.

Flory, P. J. (1962) On the Morphology of the Crystalline State in Polymers, *J. Am. Chem. Soc,* 84, 2857-2867.

Flory, P. J.; Yoon, D. Y. and Dill, K. A. (1984) The Interphase in Lamella Semicrystalline Polymers, *Macromolecules* 17, 862-868.

Glotin, M. and Mandelkern, L. (1983) On the Use of Raman-Active Longitudinal Acoustic Modes in the Study of Polyethylene Lamellar Structures, *J. Polym. Sci. Polym. Phys. Ed.* 21, 29-43.

Godshall, D.; Wilkes, G.; Krishnaswamy, R. K. and Sukhadia, A. M. (2003) Processing-Structure-Property Investigation of Blown HDPE Films Containing both Machine and Transverse Direction Oriented Lamellar Stacks, *Polymer* 44, 5397-5406.

Hahn, B.; Wendorff, J. and Yoon, D. Y. (1985) Dielectric Relaxation of the Crystal-Amorphous Interphase in Poly(Vinylidene Fluoride) and Its Blends with Poly(methylmethacrylate), *Macromolecules* 18, 718-721.

- 13 -

Hubert, L.; David, L.; Seguela, R. and Vigier, G. (2004) Small-Angle X-ray Scattering Investigation of the Deformation Processes in the Amorphous Phase of High Density Polyethylene, *Poly. Int.* 53, 582-585.

Horii, F.; Kaji, H.; Ishida, H.; Kuwabara, K.; Masuda, K. and Tai, T. (1998) Solid-State NMR Analyses of the Structure and Dynamics of Polymers in the Different States, *J. Mol. Struc.* 441, 303-311.

Hirai, A.; Horii, F. and Kitamaru, R. (1990) Studies of the Phase Structure of Poly(tetramethylene oxide) by VT/MAS ^{13}C NMR, *Macromolecule,* 23, 2913-2917.

Harris, R. K. (1986) Nuclear Magnetic Resonance Spectroscopy. Longman Scientific & Technical.

Janimak, J. J. and Stevens, G.C. (2001) Inter-Relationships between Tie-Molecule Concentrations, Molecular Characteristics and Mechanical Properties in Metallocene Catalyzed Medium Density Polyethylenes, *J. Mat. Sci.* 36, 1879-1884.

Kitamaru, R.; Horii, F. and Murayama, K. (1986) Phase Structure of Lamellar Crystalline Polyethylene by Solid-State High-Resolution ^{13}C NMR: Detection of the Crystalline-Amorphous Interphase, *Macromolecules* 19, 636-643.

Kitamaru, R.; Horii, F. and Hyon, S. H. (1977) Proton Magnetic Resonance Studies of the Phase Structure of Bulk-Crystallized Linear Polyethylene, *J. Polym. Sci.,Polym. Phys.Ed.* 15, 821-836.

Kitamaru, R.; Horii, F. and Murayama, K. (1982) *Polymer Bulletin (Berlin)* 7, 583.

Kuwabara, K.; Kaji, H. and Horii, F. (1997) Solid-State ^{13}C NMR Analysis of the Crystalline-Noncrystalline Structure for Metallocene-Catalyzed Linear Low-Density Polyethylene, *Macromolecules* 30, 7516-7521.

Kumar, S. K. and Yoon, D. Y. (1989) Lattice Model for Crystal-Amorphous Interphases in Lamellar Semicrystalline Polymers: Effects of Tight-Fold Energy and Chain Incidence Density, *Macromolecules* 22, 3458-3469.

Matsumoto, A.; Egawa, Y.; Matsumoto, T. and Horii, F. (1996) Miscibility of Polyoxymethylene Blends as Revealed by High-resolution Solid-State ^{13}C-NMR Spectroscopy, *Polymers for Advanced Technologies* 8, 250-256.

Mandelkern, L. (1990) The Structure of Crystalline Polymers, *Acc. Chem. Res.*, 23, 380-386.

Perez, E. and VanderHart, D. L. Morphological Partitioning of Ethyl Branches in Polyethylene by ^{13}C Nuclear Magnetic Resonance, *Macromolecule* 20, 78-87.

Popli, R.; Glotin, M.; Mandelkern, L. and Benson, R. S. (1984) Dynamic Mechanical Studies of α and β Relaxations of Polyethylenes, *J. Polym. Sci., Polym. Phys. Ed.* 22, 407-448.

Russell, T. P.; Ito, H. and Wignall, G. D. (1988) Neutron and X-Ray Scattering Studies on Semicrystalline Polymer Blends, *Macromolecules* 21, 1703-1709.

Spitalsky, Z. and Bleha, T. (2003) Elastic Moduli of Highly Stretched Tie Molecules in Solid Polyethylene, *Polymer,* 44, 1603-1611.

Strobl, G. R. and Hagedorn, W. (1978) Raman Spectroscopic Method for Determining the Crystallinity of Polyethylene, *J. Polym. Sci., Polym. Phys. Ed.* 16, 1181-1193.

VanderHart, D. L. and Perez, E. (1986) A ^{13}C NMR Method for Determining the Partitions of End Groups and Side Branches between the Crystalline and Noncrystalline Regions in Polyethylene, *Macromolecules* 19, 1902-1909.

Voigt-Martin, I. G.; Stack, G. M.; Peacock, A. J. and Mandelkern, L. (1989) Numerical Analysis of Lamellar Thickness Distributions, *J. Polym. Sci., Part B: Polym. Phys.* 27, 967-991.

Spiess, H. W. (2004) Advanced Solid-State Nuclear Magnetic Resonance for Polymer Science, *J. polym. Sci.: Part A: Polym. Chem.* 42, 5031-5044.

Suzaki, H.; Grebowicz, J. and Wunderlich, B. (1985) Heat Capacity of Semicrystalline, Linear Poly(oxymethylene) and Poly(oxyethylene), *Macromol. Chem.* 18, 1109-1119.

Zhang, L.; Qun, C. and Hansen, E. W. (2005) Morphology and Phase Characteristics of High-Density Polyethylene Probed by NMR Spin Diffusion and Second Moment Analyses, *Macromol. Chem. Phys.* 206, 246-257.

Zhizhenkov, V.V. and Egorov, E.A. (1984) NMR Study of the Tie-Chain Length Distribution in Oriented Polymers, *J. Polym. Sci. Poly. Phys. Ed.,* 22, 117-127.

Zhang, X. M.; Elkoun, S.; Ajji, A. and Huneault, M. A. (2004) Oriented Structure and Anisotropy Properties of Polymer Blown Films: HDPE, LLDPE and LDPE, *Polymer* 45, 217-229.

CHAPTER 3

Solid-State Nuclear Magnetic Resonance (NMR) Spectroscopy

3.1 Overview

NMR spectroscopy is a well-known and powerful technique for polymer characterization. The use of solution NMR for polymer analyses has become routine in chemistry laboratories. Usually solution NMR includes solutions, gels, dispersions, melts, etc. [Cheng and English 2002]. Because final polyethylene products are usually solids, solid-state NMR spectroscopy is the principal experimental tool to explore the morphological features of polyethylene samples. The technique is a vibrant and exciting field where many new techniques appear regularly [Schmidt-Rohr and Spiess 1996; Spiess 2004]. Solid-state NMR techniques, especially those that are relevant to this thesis are presented in this section.

3.2 Solid-State NMR Spectroscopy

3.2.1 High-Resolution Solid-State ^{13}C NMR Spectra

Solid-state ^{13}C NMR spectra usually have broad lineshapes because of chemical shielding anisotropy and dipolar couplings. Three techniques, namely, high-power proton decoupling, cross polarization (CP) and magic angle spinning (MAS), can be utilized to produce high-resolution ^{13}C spectra. ^{13}C CP/MAS NMR

spectra have been routinely used by chemists to investigate structural information of molecules.

3.2.1.1 Cross Polarization (CP)

Cross polarization (CP), usually from protons to rare spins, is an important solid-state NMR technique. The principle of the CP process is demonstrated by using the ^{13}C-^1H system. The basic concept of CP is to derive the ^{13}C magnetization from the ^1H spins by using the pulse sequence shown in Figure 3.1.
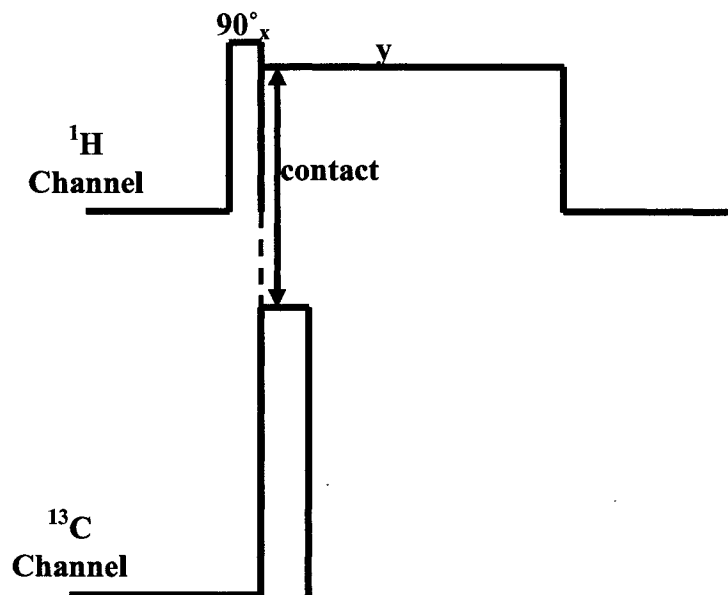
Figure 3.1 Pulse sequence used to obtain CP from ^1H to ^{13}C.

The first step is to apply a $90°$ pulse in the proton channel and then spin-lock the ^1H magnetization in the y-direction of the rotating frame. At this point the r.f. in

- 19 -

the ^{13}C channel is switched on, and the amplitude of the magnetic filed B_{1C} adjusted so that the Hartmann-Hahn matching condition [Hartmann and Hahn 1962] is fulfilled:

$$\gamma_H B_{1H} = \gamma_C B_{1C} \qquad (3\text{-}1)$$

This condition implies that in their respective rotating frames of reference the proton and carbon magnetic moments precess at equal rates and that the effective energies are comparable, thus allowing a rapid transfer of magnetization. CP takes advantage of the fact that proton spin diffusion generally causes all of the protons in a solid to have the same T_1 value, and that the proton T_1 is usually short compared to the carbon T_1 values. Because polarization is being transferred from the protons to the carbons, it is the shorter T_1 of the protons that dictates the repetition rate for signal averaging [Harris 1985].

3.2.1.2 Magic Angle Spinning (MAS)

The dipolar interactions between ^{13}C and ^{1}H and ^{13}C shielding anisotropies, which involve the geometrical factor $(3\cos^2\theta - 1)/2$, usually cause broad, featureless spectra for solid polymers. For isotropic solutions, the geometrical factor $(3\cos^2\theta - 1)$ is averaged by rapid isotropic molecular tumbling. For solids, magic angle spinning (MAS) is routinely used to remove the effect of chemical shielding anisotropy and also to assist in the removal of dipolar coupling effects. The geometrical factor $(3\cos^2\theta - 1)$ can be written as:

$$\langle 3\cos^2\theta - 1 \rangle = \frac{1}{2}(3\cos^2\beta - 1)(3\cos^2\chi - 1) \qquad (3\text{-}2)$$

- 20 -

with θ, β and χ defined in Figure 3.2. When $\beta \approx 54.7356°$, $(3\cos^2\theta - 1)=0$ for all orientations. In other words, if the sample is spun rapidly at an angle of $54.7356°$, both the dipolar interactions and the shielding anisotropies will be averaged to zero, and thus broadening will be eliminated, giving much higher resolution. This situation is referred to as MAS and $54.7356°$ is called the magic angle [Harris 1985].
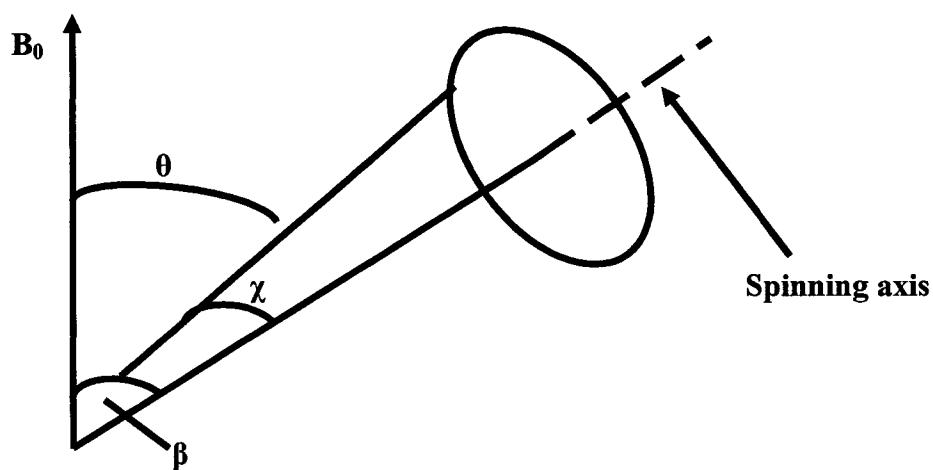
Figure 3.2 Sample spinning at an angle to the external magnetic field B_0, demonstrating the angles of θ, β and χ involved.

3.2.1.3 High-power Proton Decoupling

High-power proton decoupling is the technique which involves the double-resonance procedure of decoupling to remove the effects of dipolar coupling between proton and other nuclei. Specifically, for a ^{13}C-^{1}H system, the method consists of applying continuous irradiation of very high power at the frequency of the proton resonance. The required pulse sequence for the ^{13}C nuclei is then applied

and the ^{13}C FID acquired while continuing the ^{1}H irradiation. Because of the strength of dipolar couplings between ^{13}C and ^{1}H, very high decoupling powers are required. Note that scalar decoupling occurs at the same time. This approach is now standard for the observation of solid-state spectra of ^{13}C and other nuclei [Harris 1985].

3.2.2 Relaxation Processes

NMR relaxation parameters are very sensitive to changes in local dynamics due to the combined influence of the spectral density of the fluctuations and the inverse sixth power of the appropriate distance dependence of the dipolar interactions with mobile protons. The measurements of the relaxation times of ^{13}C nuclei in natural abundance (1.1%) have been used extensively for the study of polymers. There are several reasons for this [Bovey *et al.* 1987]:

a. ^{13}C resonances are generally well resolved in chemical shift so that separate T_1 measurements are feasible.

b. ^{13}C nuclei are spatially isolated so that mutual dipole-dipole interactions are negligible.

c. Carbon atoms are generally not at the periphery of the molecule and so only intramolecular influences need be considered.

Three relaxation processes, namely, the spin-lattice (T_1), spin-spin (T_2) and spin-lattice relaxation in the rotating frame ($T_{1\rho}$), are introduced in the following section.

- 22 -

3.2.2.1 Spin-Lattice (T_1) Relaxation

The spin-lattice relaxation time, T_1, is the relaxation of the net magnetization along the z-axis. Following a 180° pulse, the z-magnetization returns to equilibrium via purely spin-lattice relaxation, normally exponential as given by Equation (3-3):

$$M_z(t) - M_0 = [M_z(0) - M_0]\exp(-t/T_1) \qquad (3\text{-}3)$$

The inversion recovery method is the standard method for measuring T_1. The pulse sequence is:

$$[180° - \tau - 90°(FID) - T_d]_n \qquad (3\text{-}4)$$

The natural logarithm of the peak height, $S(t)$, for each peak may be plotted against τ, and thus T_1 can be found according to the following equation (provided that at long times, full recovery is achieved):

$$\ln[S(\infty) - S(t)] = \ln 2 + \ln S(\infty) - \tau/T_1 \qquad (3\text{-}5)$$

In polymer systems, T_1 is most sensitive to high-frequency molecular motions (on the order of MHz) [Fyfe 1983; Kuwabara et al. 1997]. For polyethylene, the dominant mechanism of T_1 relaxation is dipolar relaxation.

3.2.2.2 Spin-Spin (T_2) Relaxation

The spin-spin relaxation time, T_2, is the relaxation of the net magnetization in the x-y plane. The fluctuations of local magnetic field cause dynamic transitions between different energy states which result in T_2 relaxation. T_2 relaxation is also a de-phasing process, which involves no energy exchange with the lattice. In the

- 23 -

absence of external magnetic field ($\mathbf{B_0}$) inhomogeneity, a 90° pulse is followed by the T_2 relaxation, usually exponential as:

$$M_y(t) = M_y(0)\exp(-t/T_2) \qquad (3\text{-}6)$$

The measurement of T_2 usually involves the utilization of the spin-echo phenomena. A sequence known as the Carr-Purcell-Meiboom-Gill (CPMG) is often used to measure the true T_2 (without the interference of field inhomogeneity).

$$90°_x \left[-\tau - 180°_y - \tau - echo - \right]_N \qquad (3\text{-}7)$$

Every factor that affects spin-lattice relaxation will have an influence on spin-spin relaxation; moreover, for T_2 there are additional contributions from low-frequency molecular motions [Sanders and Hunter 1993]. As for T_1, dipolar relaxation is the dominant mechanism for T_2 relaxation.

3.2.2.3 Spin-Lattice Relaxation in the Rotating Frame ($T_{1\rho}$)

As discussed in 3.2.2.2, a 90° pulse is followed by T_2 relaxation. However, in another case, if the 90° pulse is phase shifted by another 90° (as illustrated in Figure 3.3), the magnetization is then be spin-locked by B_{1y}. Since the magnetization is developed by B_0, it is far larger than can be maintained by B_1 and therefore the magnetization will decay with time and this decay is referred to as spin-lattice relaxation in the rotating frame, and is frequently exponential, characterized by a time designated as $T_{1\rho}$.

$$M_y(\tau) = M_0\exp(-\tau/T_{1\rho}) \qquad (3\text{-}8)$$

- 24 -
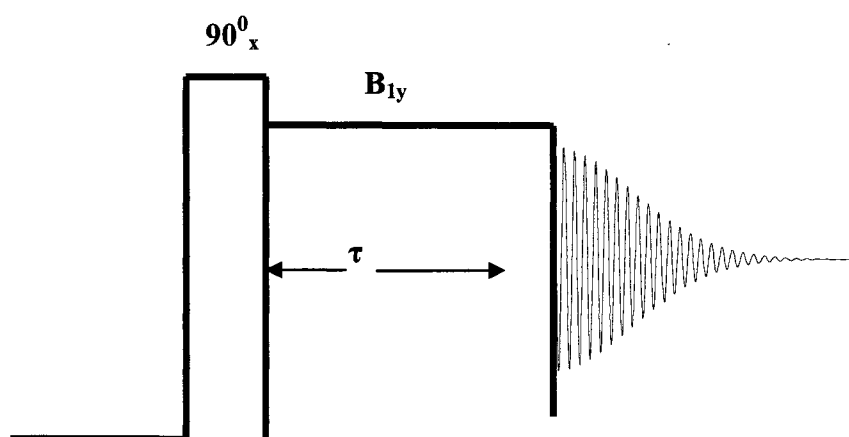
Figure 3.3 Spin-lattice relaxations in the rotating frame.

$T_{1\rho}$ is closely related to molecular motions in the order of kHz and this range of molecular motion is closely associated with mechanical relaxation behaviour, thus $T_{1\rho}$ is important in mechanical studies [Fyfe 1983]. Also proton $T_{1\rho}$ values are important for CP experiments [Duer 2004].

3.2.2.4 Summary on Relaxation Processes

T_1 measurements allow the study of fast, megahertz-order frequency molecular motion, $T_{1\rho}$ measurements provide a way to investigate the slower motions in the low- to mid-kilohertz frequency range, which may be closely associated with the mechanical relaxation behaviour of polyethylene samples, and finally T_2 values are affected by motions below the order of 10^9 Hz [Fyfe 1983]. Since different phases in polyethylene samples tend to have distinct motion frequencies, the relaxation study offers a practical way to characterize the phase structure of polyethylene [Kitamaru *et al*. 1985; Horii *et al*. 1998].

- 25 -

3.2.3 Discriminating Techniques: the Utilization of Special Pulse Sequences

Discriminating techniques are used to determine the partitioning of the branches in the crystalline and non-crystalline regions [VanderHart and Perez 1986; Perez *et al.* 1987]. In principle, techniques (the utilization of special pulse sequences) that distinguish between sites are employed to generate high-resolution ^{13}C spectra of the crystalline and non-crystalline regions separately. By observing and comparing the signal level of the branches shown in the spectra, one can determine the partitioning of the branches between the two regions. The key to discrimination lies in devising an experiment which depends on an NMR property which differs between the regions. $T_{1\rho}$ for protons is often such a property. The value of $T_{1\rho}$ for ^1H in different spatial regions may vary by an order of magnitude or more. One of such pulse sequences is introduced below.

3.2.3.1 The Delayed Contact Pulse Sequence

As illustrated in Figure 3.4, to obtain spectra of regions with longer values of $T_{1\rho}$ preferentially, an appropriate delay time, τ, can be used. During the delay time, the ^1H magnetization of regions with short $T_{1\rho}$ values will decay, so that it is not available for the cross polarization. Thus by choosing an appropriate τ value, the spectrum will be that of regions with long ^1H $T_{1\rho}$ only. This method has been employed to investigate the branch locations of polyethylene samples [Kuwabara *et al.* 1997; VanderHart and Perez 1986; Perez *et al.* 1987].

- 26 -
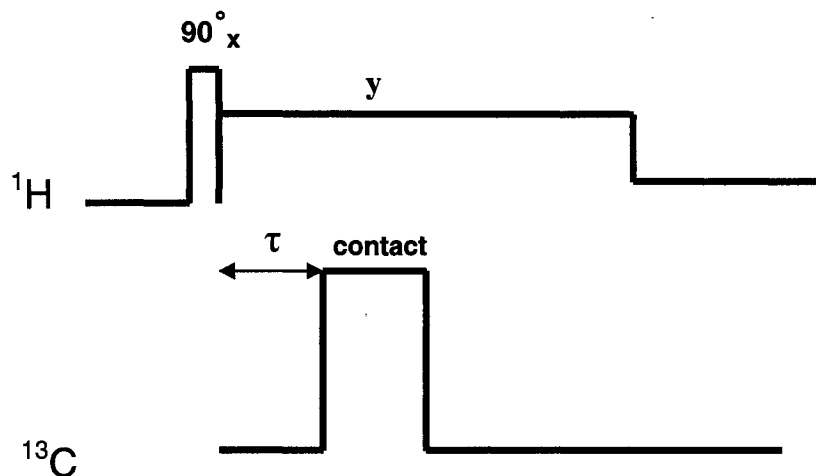
Figure 3.4 The delayed contact pulse sequence.

3.3 References

Bovey, F. A.; Jelinski, L. and Mirau, P. A. (1987) Nuclear Magnetic Resonance Spectroscopy, Academic Press Inc., San Diego, USA.

Cheng, H. N. and English, A. D. (2002) NMR Spectroscopy of Polymers in Solution and in the Solid State, American Chemical Society, Washington DC, USA.

Duer, M. J. (2004) Introduction to Solid-State NMR Spectroscopy, Blackwell Publishing Ltd., Oxford, UK.

Fyfe, C. A. (1983) Solid State NMR for Chemists, C.F.C. Press, Guelph, Ontario, Canada.

Harris, R. K. (1985) Nuclear Magnetic Resonance Spectroscopy, A Physicochemical View, Longman, London, UK.

Horii, F.; Kaji, H.; Ishida, H.; Kuwabara, K.; Masuda, K. and Tai, T. (1998) Solid-State NMR Analyses of the Structure and Dynamics of Polymers in the Different States, *J. Mol. Struc.* 441, 303-311.

Hartmann, S. R. and Hahn, E. L. (1962) Nuclear Double Resonance in the Rotating Frame, *Phys. Rev.* 128, 2042-2053.

Kuwabara, K.; Kaji, H.; Horii, F.; Bassett, D. C.; Olley, R. H. (1997) Solid-State ^{13}C NMR Analyses of the Crystalline-Noncrsytalline Structure for Metallocene-Catalyzed Linear Low-Density Polyethylene, *Macromolecules* 30, 7516-7521.

Kitamaru, R.; Horii, F. and Murayama, K. (1985) Phase Structure of Lamella Crystalline Polyethylene by Solid-State High-Resolution ^{13}C NMR: Detection of the Crystalline-Amorphous Interphase, *Macromolecules* 19, 636-643.

Perez, E.; VanderHart, D. L.; Crist Jr., B. and Howard, P.R. (1987) Morphological Partitioning of Ethyl Branches in Polyethylene by ^{13}C Nuclear Magnetic Resonance, *Macromolecules* 20, 78-87.

Schmidt-Rohr, K. and Spiess, H. W. (1996) Multidimensional Solid-State NMR and Polymers, Academic Press Inc., San Diego, USA.

Sanders, J. K. and Hunter, B. K. (1993) Modern NMR Spectroscopy A Guide for Chemists, Oxford University Press Inc., New York, USA.

Spiess, H. W. (2004) Advanced Solid-State Nuclear Magnetic Resonance for Polymer Science, *J. Polym. Sci.: Part A: Polym. Chem.* 42, 5031-5044.

VanderHart, D. L. and Perez, E. (1986) A ^{13}C NMR Method for Determining the Partitioning of End Groups and Side Branches Between the Crystalline and Noncrystalline Regions in Polyethylene, *Macromolecules* 19, 1902-1909.

CHAPTER 4

Morphology of Ziegler-Natta and Single-Site Linear Low-Density Polyethylenes: Insights from Solid-State ^{13}C NMR Spectroscopy, Fuming Nitric Acid Etching and GPC

4.1 Introduction

It has long been recognized that single-site linear low-density polyethylene (ss-LLDPE) possesses a higher degree of intermolecular branch content homogeneity than LLDPE synthesized with the use of Ziegler-Natta catalysts (ZN-LLDPE). It is generally believed that such a difference leads to different morphological features for the two types of LLDPEs, which in turn give rise to different mechanical performances. For example, ZN-LLDPE shows a higher tear resistance but a lower dart impact resistance than ss-LLDPE [Guichon *et al.* 2003].

The morphology of polyethylene can be investigated by various experimental methods. For example, solid-state ^{13}C nuclear magnetic resonance (NMR) spectroscopy was used to study the phase structure of polyethylenes [Kitamaru *et al.* 1986; Shimizu *et al.* 1995; Horii *et al.* 1998; Kuwabara *et al.* 1997; Earl and VanderHart 1979]. Solid-state ^{13}C NMR techniques are powerful for the elucidation of morphological features of polyethylenes, especially those related to the crystalline-amorphous interphase. Fuming nitric acid (FNA) etching of polyethylene samples followed by gel permeation chromatography (GPC) measurements was used to study the size and size distribution of polyethylene crystalline lamella [Cook *et al.* 2000; Capaccio and Ward 1981; 1982; Pascale and Rentzepis 1965].

- 30 -

The combination of NMR techniques with other experimental methods, such as transmission electronic microscopy (TEM), can provide greater versatility in the morphological study of polyethylenes. In this work, solid-state NMR techniques, together with FNA etching and GPC measurements, were performed to investigate the morphological features of ss- and ZN-LLDPEs. The combination of these methods enables us to reveal more detailed structural information of polyethylenes. In particular, the morphological features of the interphase were investigated.

4.2 Experimental Section

4.2.1 Materials

Two LLDPE samples (one ss-LLDPE and one ZN-LLDPE) with comparable characteristics were obtained from Nova Chemicals Corp. in Calgary, Canada. The characteristics are listed in Table 4.1.

Table 4.1 Characteristics of ss- and ZN-LLDPEs

Resin	M_n	M_w	PDI[a]	Melt Index (dg/min)	Density (g/cm^3)	Branch Content [b]
ZN-LLDPE	26,400	116,160	4.4	0.65	0.9229	12.7
ss-LLDPE	34,800	104,400	3.0	0.68	0.9196	11.3

[a] Polydispersity
[b] Number of branches per 1,000 backbone carbons.

- 31 -

4.2.2 FNA Etching

Samples to be etched were placed in sealed glass bottles which were then placed in an oil bath at a temperature of 60 °C. The samples were allowed to degrade with excess fuming nitric acid for 1, 2 and 30 days, respectively. After etching, the residue of the sample was filtered and washed several times with distilled water and then immersed into distilled water and rinsed for 24 h. The cleansed sample was then dried overnight in a vacuum oven at room temperature. The dried etched samples were stored in glass bottles for GPC and NMR analyses.

4.2.3 GPC Measurements

GPC measurements were performed to determine the average molecular weight and weight distribution of the etched samples. GPC experiments at 145 °C were performed on an Alliance GPCV 2000 using 1,2,4-trichlorobenzene as the solvent. Waters HT6E columns with a guard coil were used. The flow rate was set to 1.0 ml/min. Linear polyethylene samples with narrow molecular weight distribution were used as standards for the calibration.

4.2.4 Solid-State ^{13}C NMR Analyses

Solid-state ^{13}C NMR analyses were performed on a Chemagnetics CMX Infinity 200 spectrometer, operating at 200.15 MHz for ^{1}H and 50.32 MHz for [13]C. Samples were packed in 7.5 mm o.d. zirconia rotors. Spectra for the original and etched ss- and ZN-LLDPEs were obtained at room temperature with the standard

cross-polarization (CP) pulse sequence. The contact time for the cross-polarization was 1 ms and the magic angle spinning (MAS) rate was set to 3 kHz. ^{13}C chemical shifts were referenced to tetramethylsilane (Me$_4$Si, δ_{iso} = 0) by setting the isotropic high-frequency peak of adamantane to 38.56 ppm [Earl and VanderHart 1982].

Because spectra obtained with CP are not quantitative, fully-relaxed ^{13}C spectra were obtained with single-pulse excitation and a 1,500 s delay to allow complete relaxation of the ^{13}C nuclei. The degree of crystallinity for each of the LLDPEs was determined from their fully-relaxed ^{13}C NMR spectra by calculating the relative intensities of the peaks.

^{13}C spin-lattice (T_1) relaxation times were measured by the CPT1 pulse sequence [Torchia 1978]. ^{13}C spin-spin (T_2) relaxation times were measured by the modified spin-echo pulse sequence [Hirai et al. 1990] with two-pulse phase modulation (TTPM) decoupling [Bennett et al. 1995] only during the acquisition time. The pulse sequence is shown in Figure 4.1.
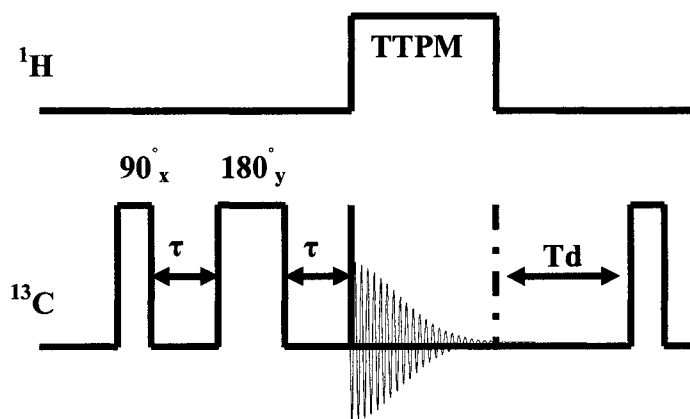
Figure 4.1 The modified spin-echo pulse sequence with TTPM decoupling used for T_2 measurements.

4.3 Results and Discussion

Two ^{13}C NMR spectra for ss-LLDPE are shown in Figure 4.2. Two peaks are observed from both the CP and fully-relaxed spectra. The peak at 32.9 ppm is assigned to the orthorhombic crystalline component, whereas the broad peak centered at 31.0 ppm is assigned to the non-crystalline components [Kitamaru *et al.* 1986; Shimizu *et al.* 1995; Horii *et al.* 1998; Kuwabara *et al.* 1997; Earl and VanderHart 1979]. To obtain more morphological information, measurements of ^{13}C T_1 and T_2 relaxation times were performed.

a)

b)

| 45 | 40 | 35 | 30 | 25 | 20 | 15 | 10 |

δ / ppm
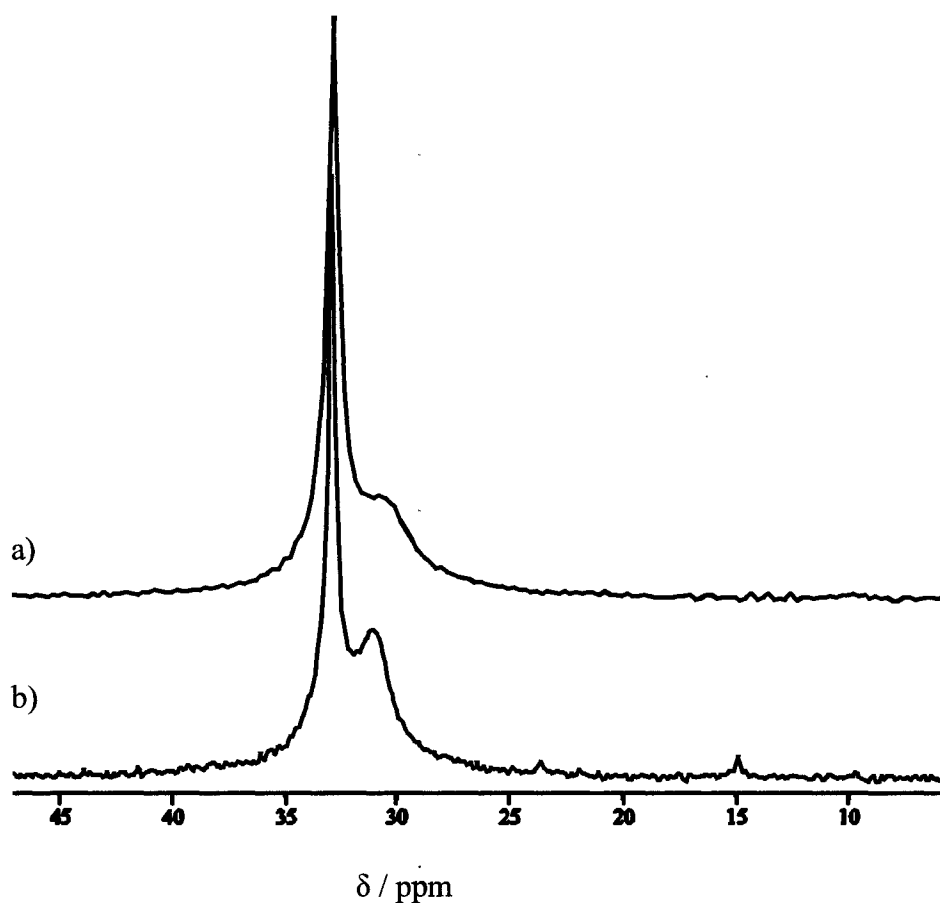
Figure 4.2 ^{13}C NMR spectra for ss-LLDPE: a) CP; b) Fully-relaxed.

- 34 -

In Figure 4.3 (a), the magnetization of the crystalline component (the peak at 32.9 ppm) of ss-LLDPE, which was measured by the CPT1 pulse sequence [Torchia 1978], is plotted against the decay time. Figure 4.3 (b) shows the natural logarithmic peak intensities versus the decay time. The experimental data could not be fit to a single-exponential decay, suggesting that ^{13}C nuclei with different T_1 relaxation times are contributing to the intensity of this peak. In fact, the data can be fit by a three-decay model as:

$$y = A_1 \exp(-t/T_{1,a}) + A_2 \exp(-t/T_{1,b}) + A_3 \exp(-t/T_{1,c}) + y_0 \qquad (4.1)$$

The T_1 relaxation behaviours of the three components are shown in Figure 4.3 (b). The solid line in Figure 4.3 (a), which is the composite fit curve of the three components, obtained by the least-square method, is in good agreement with the experimental data. As a result, three components with different T_1 values were resolved for the crystalline peak of ss-LLDPE. Likewise, three components with different T_1 values were determined for the crystalline component of ZN-LLDPE. The results are summarized in Table 4.2. These observations are consistent with the results found by other studies [Kitamaru *et al.* 1986; Horii *et al.* 1998; Kuwabara *et al.* 1997].

^{13}C T_1 values for the non-crystalline components of ss- and ZN-LLDPEs were also measured; the data can be fit with a single T_1 value (see Table 4.2), which indicates that the non-crystalline components behave homogeneously with respect to motions in the MHz frequency range.

- 35 -
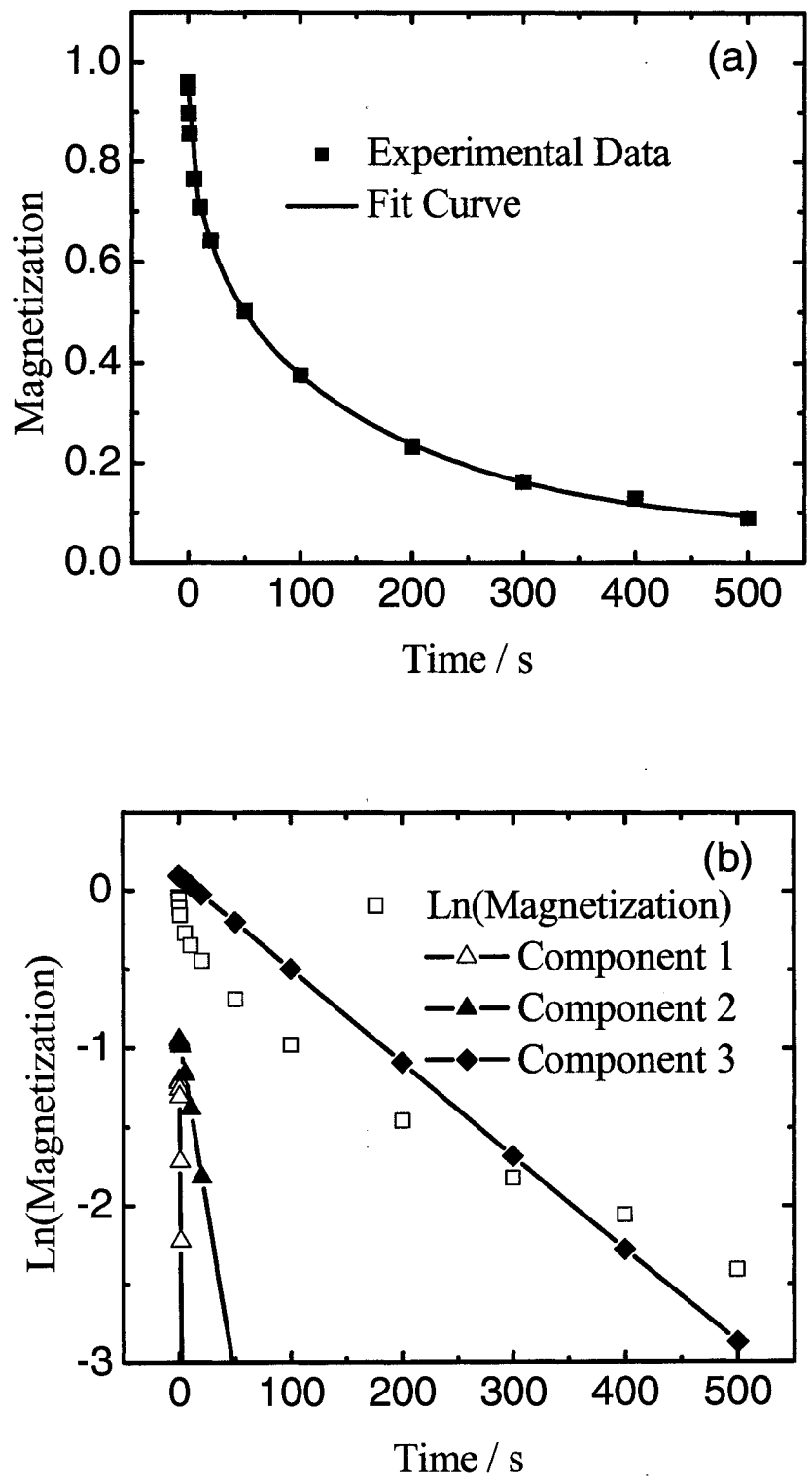
Figure 4.3 ^{13}C T_1 relaxation for the crystalline component of ss-LLDPE.

Table 4.2 Measured relaxation times (T_1 and T_2) and calculated mass fractions of various phases in ss- and ZN-LLDPEs.

Sample	Parameter		
	T_1 (s)	T_2 (ms)	Mass fraction [a]
ss-LLDPE			
Crystalline	168.6, 23.1, 1.0	N/A	0.43
Interfacial	0.6	0.064	0.47
Amorphous	0.6	2.1	0.10
ZN-LLDPE			
Crystalline	214.6, 16.9, 0.7	N/A	0.54
Interfacial	0.5	0.072	0.35
Amorphous	0.5	2.4	0.11

[a] It was estimated that errors associated with these results are within ±0.05

The ^{13}C T_2 relaxation process for the non-crystalline peak (31.0 ppm) of ss-LLDPE, which is measured by the modified spin-echo pulse sequence with TTPM decoupling, is shown in Figure 4.4 (a). Figure 4.4 (b) shows the natural logarithmic peak intensities versus the evolution time. The trend of the experimental data is not a straight line; therefore, the data cannot be fit by a single-component model. In fact, a two-decay model was required to fit the observed data, suggesting that two components with different ^{13}C T_2 relaxation behaviours were included in the non-crystalline region.

$$y = A_1 \exp(-t/T_{2,a}) + A_2 \exp(-t/T_{2,b}) + y_0 \qquad (4.2)$$
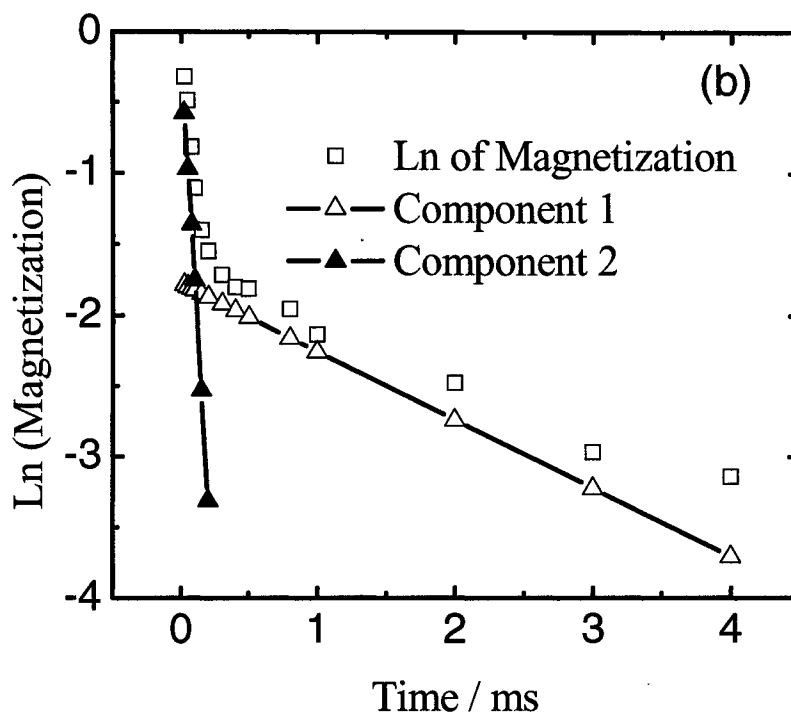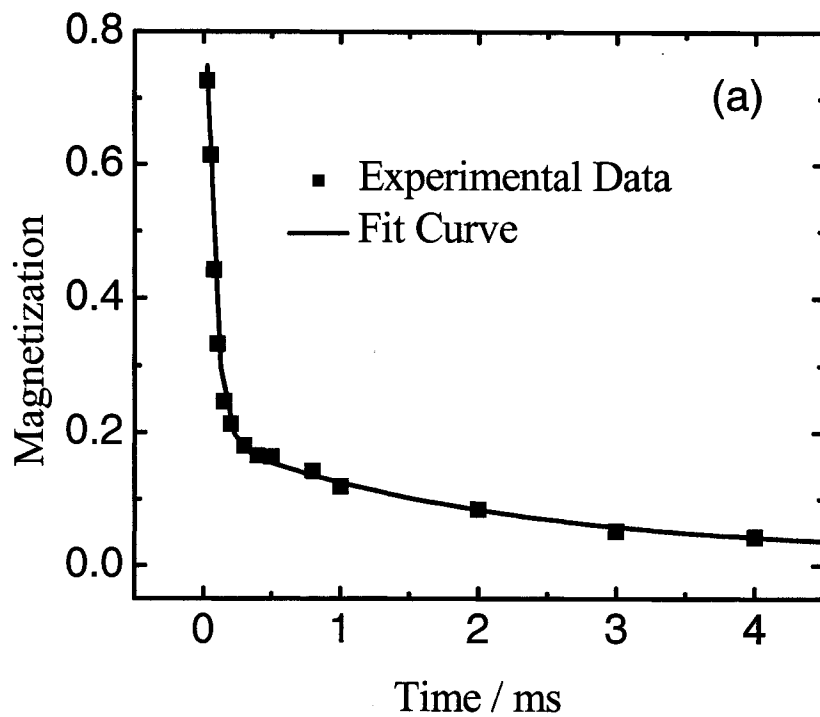
Figure 4.4 ^{13}C T_2 relaxation for the non-crystalline component of ss-LLDPE.

By the least-square fitting, A_1, $T_{2,a}$, A_2 and $T_{2,b}$ were determined. The two components with very different T_2 vales are shown in Figure 4.4 (b). The composite fit curve shown in Figure 4.4 (a) is in good accord with the experimental data. During the ^{13}C T_2 study, when τ (as shown in Figure 4.1) longer than 0.5 ms (during which the component with the shorter T_2 value is totally relaxed), the remaining lineshapes of the spectra are closely approximated by a Lorentzian form, suggesting the component with much longer T_2 value has liquid-like chain motions. Therefore, the component with T_2 =2.1 ms was assigned to the amorphous phase. In contrast, the component with T_2 =64 µs, which has much reduced chain motions, was assigned to the crystalline-amorphous interphase. These assignments were consistent with those reported elsewhere [Kitamaru *et al.* 1986; Horii *et al.* 1998; Kuwabara *et al.* 1997]. Similarly, two components with very different T_2 values were determined for ZN-LLDPE. It was also observed that the T_2 value for the interphase of ss- and ZN-LLDPEs is close, indicating that the molecular mobility within the interphase is similar for both LLDPEs. Because A_1 and A_2 are directly related to quantities of ^{13}C nuclei in these two regions, the mass ratio of the interphase to the amorphous phase was also determined from T_2 measurements.

The degree of crystallinity was calculated from the relative intensities of the crystalline and non-crystalline peaks of the fully-relaxed ^{13}C spectra of MAS ss- and ZN-LLDPE samples. It was found that the degree of crystallinity for ss-LLDPE is 0.43, whereas that for ZN-LLDPE is 0.54. This is consistent with the fact that ZN-LLDPE has a higher solid-state density than ss-LLDPE (see Table 4.1). It was also

- 39 -

observed that the mass fraction for the interphase of ss-LLDPE is 0.47, while that for ZN-LLDPE is 0.35. The results are summarized in Table 4.2.

FNA treatments of ss- and ZN-LLDPEs, followed by GPC and solid-state ^{13}C NMR analyses, were performed to determine the size and size distribution of the crystalline lamella. Figure 4.5 shows the molecular weight distribution of the etched ss-LLDPE samples. (Data of ZN-LLDPE is not shown as it resembles the curves shown in Figure 4.5). It demonstrates that after one day of etching the molecular weight was greatly reduced due to the quick removal of the amorphous component. However, the etching rate slows down with time. It is known that following the removal of the amorphous component, the acid will attack the lateral surfaces of the crystals at a much slower etching rate. The distribution curve of the 2-day etched sample is close to that of the 30-day etched one except the small shoulder on the high molecular weight side. The presence of the small shoulder is because the oxidizing acid needs time to completely diffuse into the sample thus allowing homogeneous chain scission to occur. Based on these curves, it was assumed that 30-day etching is the right condition for studying the lamella size and size distribution, in which the interfacial and amorphous parts are removed whereas the crystalline component remains undamaged.
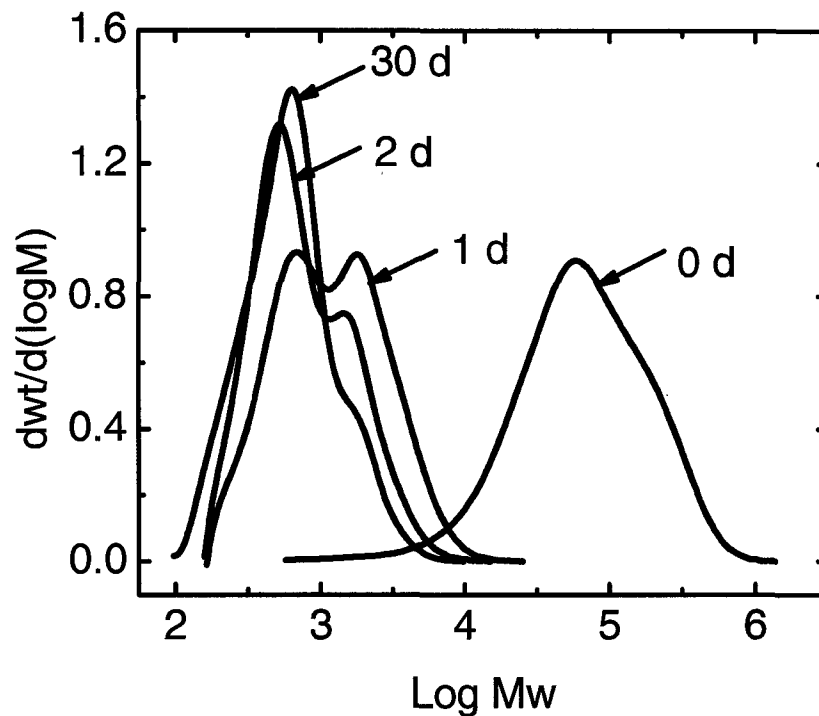
Figure 4.5 GPC chromatograms of etched ss-LLDPEs

To test the validity of the assumption, two questions were addressed. The first question is: is 30-day etching long enough to remove the non-crystalline components? We obtained high-resolution CP ^{13}C NMR spectra of the 30-day etched samples to answer this question. As shown in Figure 4.6, only the crystalline peak remains, indicating that the 30-day treatment removed the interfacial and amorphous components. The second question is: is 30-day etching too long that part of the crystalline component has also been damaged? To answer this, the trend of the lamella stem length change of the degraded samples was monitored. The sizes of the crystalline lamella for ss- and ZN-LLDPEs were calculated by using the following model: the C-C bond length in orthorhombic crystalline lamella is 1.534 Å and the CCC angle is approximately 110 degrees [Miao ea al. 1996; Montanari et al. 1998].

- 41 -

The results are summarized in Table 4.3. It was observed that the weight average chain lengths changed from 152 Å to 92 Å and 233 Å to 97 Å for ss- and ZN-LLDPE, respectively, when the etching time was varied from 1 day to 2 days. However, from 2-day to 30-day etching, the weight average chain lengths were only reduced slightly. We feel justified to conclude that even if damage occurred, it was negligible. Therefore, the average lamella stem length and length distribution can be obtained from the 30-day etched samples. As shown in Table 4.3, the average lamella stem length for ZN-LLDPE is 82 Å, whereas that for ss-LLDPE is 73 Å. This is in agreement with the results observed for the degree of crystallinity of these two samples. It is concluded that with similar sample characteristics, ZN-LLDPE has a higher degree of crystallinity and larger crystalline lamella than ss-LLDPE.

a)

b)

δ / ppm
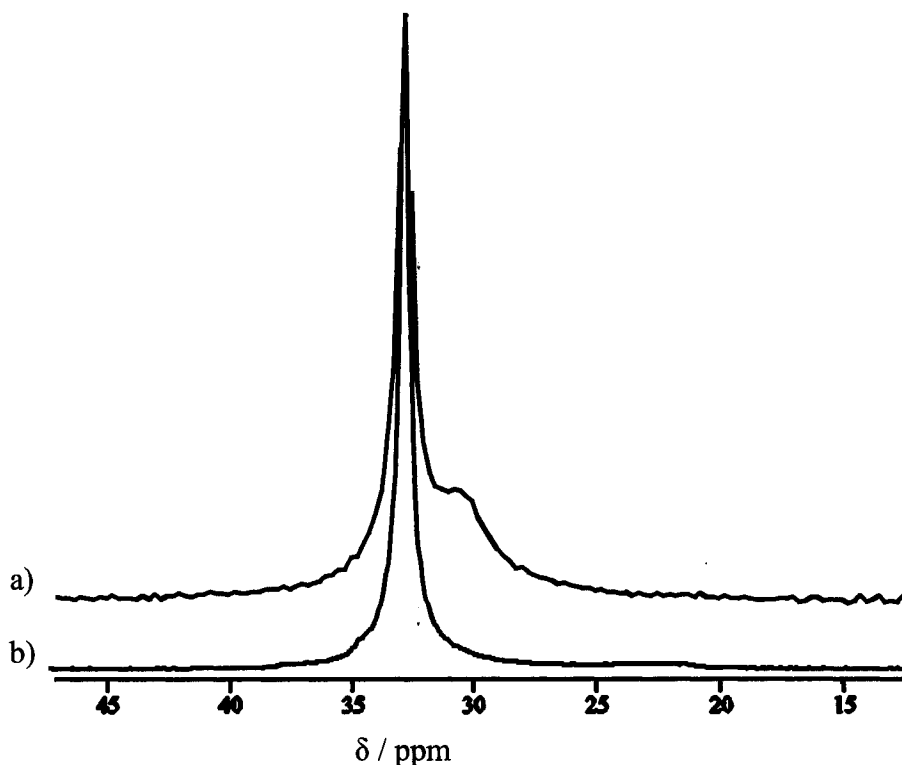
Figure 4.6 CP ^{13}C NMR spectra of the original (a) and 30-day etched (b) ss-LLDPE.

- 42 -

The length distribution of the lamella can also be derived from the molecular weight distribution of the 30-day etched samples. As shown in Table 4.3, after 30-day etching, the polydispersity indices (PDI) for both samples are close to 1.7, which means that the size distribution of the lamella is fairly narrow. It has been reported PDI of the crystalline component is in the range of 1.5~1.7 [Capaccio and Ward 1981; 1982]. Information about the lamella length distribution is of great value to the study of crystallization kinetics [Mandelkern 1986].

Table 4.3 Molecular weight averages and the corresponding average lamellar lengths

sample	t_e (days)	M_n	M_w	M_w/M_n	L_n (Å)	L_w (Å)
ss-LLDPE	1	831	1692	2.04	75	152
	2	576	1030	1.79	52	92
	30	474	812	1.71	43	73
ZN-LLDPE	1	1147	2596	2.26	103	233
	2	609	1083	1.78	55	97
	30	505	912	1.80	45	82

The interphase is defined as a transitional region where the ordered crystalline conformation gradually changes to the disordered amorphous state. The average thickness of the interfacial region can be determined from the average thickness of the crystalline lamella and the volume ratio of the crystalline phase to the interphase. Because the chain conformations in the interfacial region are close to

those in the crystalline region, it was assumed that the volume ratio of the interphase to the crystalline phase is close to the mass ratio of these two phases. As a result, the average thickness of the interfacial region for ss-LLDPE was estimated to be 39 Å; that for ZN-LLDPE is 26 Å. This is in agreement with the results of mass fractions determined for the interphase of ss- and ZN-LLDPEs. It was concluded that with similar sample characteristics, ss-LLDPE has a higher mass fraction and larger thickness for the interphase than ZN-LLDPE. The larger interfacial zone for ss-LLDPE compared to ZN-LLDPE is different from the results obtained elsewhere [Kuwabara *et al.* 1997].

4.4 Summary

The morphological features of ss- and ZN-LLDPEs were investigated by solid-state ^{13}C NMR, FNA etching and GPC. The following summarizes our conclusions.

(1) ^{13}C T_1 and T_2 relaxation time measurements of the ss- and ZN-LLDPEs reveal the existence of three phases, namely, the crystalline phase, the interphase and the amorphous phase.

(2) ZN-LLDPE shows a higher degree of crystallinity and thicker crystalline lamella than ss-LLDPE.

(3) ss-LLDPE shows a higher mass fraction and larger thickness for the interphase than ZN-LLDPE.

(4) The combination of solid-state ^{13}C NMR spectroscopy, FNA etching and GPC is capable of obtaining detailed structural information about polyethylene.

4.5 References

Bennett, A.E.; Rienstra, C.M.; Auger, M.; Lakshmi, K.V. and Griffin, R.G. (1995) Heteronuclear Decoupling in Rotating Solids, *J. Chem. Phys.* 103, 6951-6958.

Cook, J.T.E.; Klein, P.G.; Ward, I.M.; Brain, A.A.; Farrar, D.F. and Rose, J. (2000) The Morphology of Nascent and Moulded Ultra-High Molecular Weight Polyethylene. Insights from Solid-State NMR, Nitric Acid Etching, GPC and DSC, *Polymer* 41, 8615-8623.

Capaccio, G. and Ward, I.M. (1981) Structural Studies of Ultrahigh-Modulus Linear Polyethylene Using Nitric Acid Etching and Gel Permeation Chromatography. I. Determination of the Crystal Size Distribution, *J. Polym. Sci.: Polym. Phys. Ed.* 19, 667-675.

Capaccio, G. and Ward, I.M. (1982) Structural Studies of Ultrahigh-Modulus Polyethylene Using Nitric Acid Etching and Gel Permeation Chromatography. II. Influence of Polymer Molecular Weight, Draw Temperature, and Annealing, *J. Polym. Sci.: Polym. Phys. Ed.* 20, 1107-1128.

Earl, W.L. and VanderHart, D.L. (1982) Measurement of ^{13}C Chemical Shifts in Solids, *J. Magn. Reson.* 48, 35-42.

Earl, W.L. and VanderHart, D.L. (1979) Observations in Solid Polyethylenes by Carbon-13 Nuclear Magnetic Resonance with Magic Angle Sample Spinning, *Macromolecules* 12, 762-767.

Flory, P. J. (1962) On the Morphology of the Crystalline State in Polymers, *J. Am. Chem. Sci.* 84, 2857-2867.

Flory, P.J.; Yoon, D.Y. and Dill, K.A. (1984) The Interphase in Lamellar Semicrystalline Polymers, *Macromolecules* 17, 862-868.

Guichon, O.; Seguela, R.; David, L. and Vigier, G. J. (2003) Influence of the Molecular Architecture of Low-Density Polyethylene on the Texture and Mechanical Properties of Blown Films, *J. Polym. Sci., Part B: Polym. Phys.* 41, 327-340.

Horii, F.; Kaji, H.; Ishida, H.; Kuwabara, K.; Masuda, K. and Tai, T. (1998) Solid-State NMR Analyses of the Structure and Dynamics of Polymers in the Different States, *J. Mol. Struc.* 441, 303-311.

Hirai, A.; Horii, F.; Kitamaru, R.; Fatou, J.G. and Bello, A. (1990) Studies of the Phase Structure of Poly(tetramethylene oxide) by VT/MAS ^{13}C NMR, *Macromolecules* 23, 2913-2917.

Kitamaru, R.; Horii, F. and Murayama, K. (1986) Phase Structure of Lamellar Crystalline Polyethylene by Solid-State High-Resolution ^{13}C NMR: Detection of the Crystalline-Amorphous Interphase, *Macromolecules* 19, 636-643.

Kuwabara, K.; Kaji, H.; Horii, F.; Bassett, D. C. and Olley, R. H. (1997) Solid-State ^{13}C NMR Analyses of the Crystalline-Noncrystalline Structure for

Metallocene-Catalyzed Linear Low-Density Polyethylenes, *Macromolecules* 30, 7516-7521.

Miao, M. S.; Van Camp, P. E.; Van Doren, V. E.; Ladik, J. J. and Mintmire, J. W. (1996) Conformation and Electronic Structure of Polyethylene: A Density-Functional Approach, *Physical Review B* 54, 10430-10435.

Montanari, B.; Ballone, P. and Jones, R. O. (1998) Density Functional Study of Molecular Crystals: Polyethylene and a Crystalline Analog of Bisphenol-A Polycarbonate, *J. Chem. Phys.* 108, 6947-6951.

Mandelkern, L. (1990) The Structure of Crystalline Polymers, *Acc. Chem. Res.* 23, 380-386.

Pascale, J. V. and Rentzepis, P. M. (1965) Response of Polyethylene to Acid Etching *J. Appli. Polym. Sci.* 9, 2641-2649.

Shimizu; Y.; Harashina, Y.; Sugiura, Y. and Matsuo, M. (1995) Morphology and Molecular Mobility of Several Kinds of Polyethylene Specimens by ^{13}C Solid-State NMR and X-ray Diffraction Techniques, *Macromolecules* 28, 6889-6901.

Torchia, D. A. (1978) The Measurement of Proton-Enhanced Carbon-13 T_1 Values by a Method Which Suppresses Artifacts, *J. Magn. Reson.* 30, 613-617.

CHAPTER 5

Phase Structure of HDPE Films and Branch Locations in LLDPEs

5.1 Introduction

In this chapter, further utilization of the solid-state NMR techniques on solving morphological features of polyethylene is described. Two subdivisions will be covered, namely the determination of the phase structure for HDPE films; and the clarification of the locations of the short-chain branches for LLDPE resins.

The phase structure of HDPE bulk samples was investigated by Kitamaru *et al.*[1986]. Four phases were reported, namely, the monoclinic crystalline, orthorhombic crystalline, amorphous, and crystalline-amorphous interfacial phases. The phase structure of HDPE blown films has not been extensively studied. In this chapter, the elucidation of the phase structure of HDPE blown films by the procedures which were used to study the phase structure of LLDPEs is described.

The location of the branches is also an important feature of the solid state morphology of LLDPE. It is known that under equilibrium conditions, the CH_3 groups are readily incorporated into the crystalline region, while branches longer than two carbons are excluded from the crystalline region [VanderHart and Perez 1986; Perez *et al.* 1987; Alamo *et al.* 1984; Alamo and Mandelkern 1989]. On the other hand, the partitioning of the short-chain branches between the interfacial and amorphous regions is not clear yet. In this chapter, the clarification of branch locations for ss-LLDPE-M2 and ZN-LLDPE-A2 is presented.

- 48 -

5.2 Experimental Section

5.2.1 Materials

HDPE films and LLDPE resins used in this study were obtained from NOVA Chemicals Corp., Calgary, Canada. The characteristics of the samples are shown in Table 5.1 and Table 5.2, respectively.

Table 5.1 Characteristics of HDPE films used

Films	Density (g/cm^3)	MI [a] (dg/min)	M_n	M_w	M_z	PDI [b]	Branch Content [c]
04-07885	0.9591	1.23	18,800	109,200	427,900	5.81	Nil
04-08134	0.9646	7.05	15,200	60,100	136,300	3.95	Nil
04-08135	0.9619	7.04	15,500	61,100	141,900	3.94	Nil

[a] Melt Index
[b] Polydispersity index
[c] Per 1,000 backbone carbons

Table 5.2 Characteristics of bulk LLDPEs used

Resin	M_n	M_w	PDI [a]	MI (dg/min)	Branch Content [b]
ZN-LLDPE-A2	17,300	105,530	6.1	1.02	35.0
ss-LLDPE-M2	25,700	69,390	2.7	3.2	30.4

[a] Polydispersity index
[b] Per 1,000 backbone carbons

5.2.2 Solid-State ^{13}C NMR Analyses

The solid-state ^{13}C NMR techniques used to solve the phase structure of ss- and ZN-LLDPEs, as discussed in Chapter 4, were applied to HDPE films without any modifications.

The partitioning of the hexyl branches between the interfacial and amorphous regions of LLDPE samples was determined by measuring the mass ratio of the CH carbons in the interfacial region to those in the amorphous region. This ratio was determined from the study of the T_2 values of the CH carbons at the branching sites. By comparing this ratio with the one of the interphase to the amorphous phase, one can determine how the branches distribute.

5.2.3 DSC Measurements

A differential scanning calorimeter (DSC) 2910 (TA Instruments) equipped with Thermal Analyst 2200 software was used to determine the degree of crystallinity of the HDPE films. DSC scans were obtained using a heating rate of 20°C/min. Samples with masses in the range of 6-10 mg were used. The instrument was calibrated with high-purity indium standards.

5.3 Results and Discussion

5.3.1 The Phase Structure of HDPE Films

Both the CP and fully-relaxed ^{13}C NMR spectra of HDPE film 04-07885 are shown in Figure 5.1. Similar to the spectra of LLDPEs shown in Chapter 4, there are two peaks at 32.9 ppm and 31.0 ppm, corresponding to the orthorhombic crystalline and non-crystalline components, respectively. Distinct from the spectra of LLDPEs,

- 50 -

a peak at 34.4 ppm, attributed to a monoclinic crystalline phase, is observed for HDPE films. The presence of the monoclinic crystalline component is due to the mechanical deformation of orthorhombic crystalline components. The orthorhombic and monoclinic structures only differ in the way the molecules are packed in the unit cells [Young and Lovell 1991]. This observation is consistent with the results observed by others [Kitamaru *et al.* 1986; Shimizu *et al.* 1995]. The degree of crystallinity of the film was determined by calculating the relative intensities of the three peaks shown in the fully-relaxed ^{13}C NMR spectrum of an MAS sample. The degree of crystallinity of the film was also determined by DSC measurements (Figure 5.2). It was found that these two results are in good accordance (See Table 5.3).
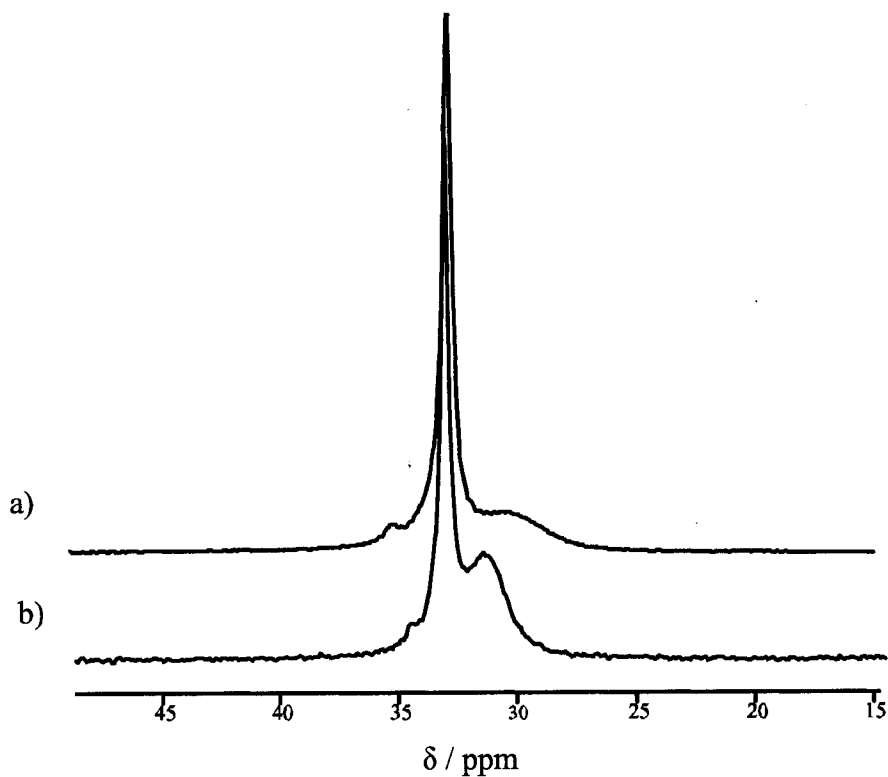
Figure 5.1 ^{13}C NMR spectra of HDPE film 04-07885: a) CP; b) Fully-relaxed.

- 51 -
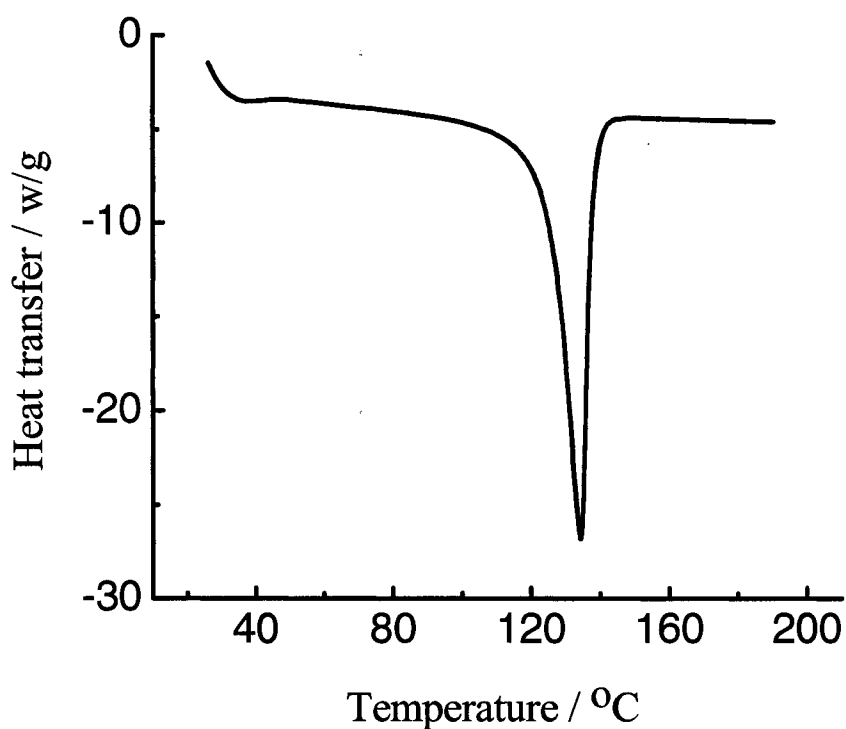
Figure 5.2 DSC scan for HDPE film 04-07885

Table 5.3 Chemical shifts, T_1, T_2 and mass fractions of the four phases of HDPE film 04-07885.

Peak	Chemical shift (ppm)	T_1 (s)	T_2 (ms)	Mass fraction (%)	Degree of Crystallinity
1 (Monoclinic)	34.4	NA	NA	1.6	0.77 [a]
2 (Orthorhombic)	32.9	2.0 , 44.6, 256.7	NA	81.3	0.829 [b]
3 (Interfacial)	31.0	0.5	0.026	14.1	
4 (Amorphous)	31.0	0.5	4.6	3.0	

[a] by DSC
[b] by solid-state ^{13}C NMR

- 52 -

In Figure 5.3 the magnetization of the orthorhombic crystalline component (the peak at 32.9 ppm) of HDPE film 04-07885, which was measured by the CPT1 pulse sequence [Torchia 1978], is plotted against the decay time to determine the T_1 values. Similar to LLDPEs, three components with different T_1 values were resolved.

The ^{13}C T_1 value for the non-crystalline peak (31 ppm) of HDPE film 04-07885 was also measured. The data can be fit with a single T_1 value (see Table 5.3), which indicates that the non-crystalline region behaves homogeneously with respect to motion in the MHz frequency range.
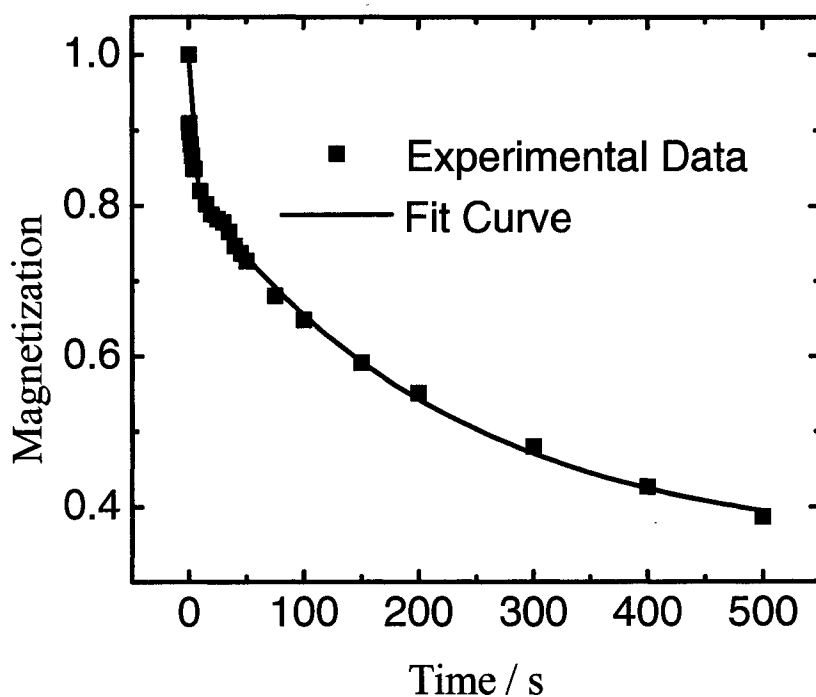
Figure 5.3 ^{13}C T_1 relaxation for the orthorhombic crystalline component of HDPE film 04-07885.

The ^{13}C T_2 relaxation process for the non-crystalline peak (31 ppm) of HDPE film 04-07885 is shown in Figure 5.3. Likewise, a two-decay model was required to fit the observed data, suggesting that two components with different ^{13}C T_2 values were included in the non-crystalline region. Similar to the assignments made to the LLDPEs, the component with T_2 =26 μs was assigned to the interphase and the one with T_2 =4.6 ms to the amorphous phase. The mass ratio of the interphase to the amorphous phase was also determined from the T_2 measurements. The mass fractions of the four phases are summarized in Table 5.3.
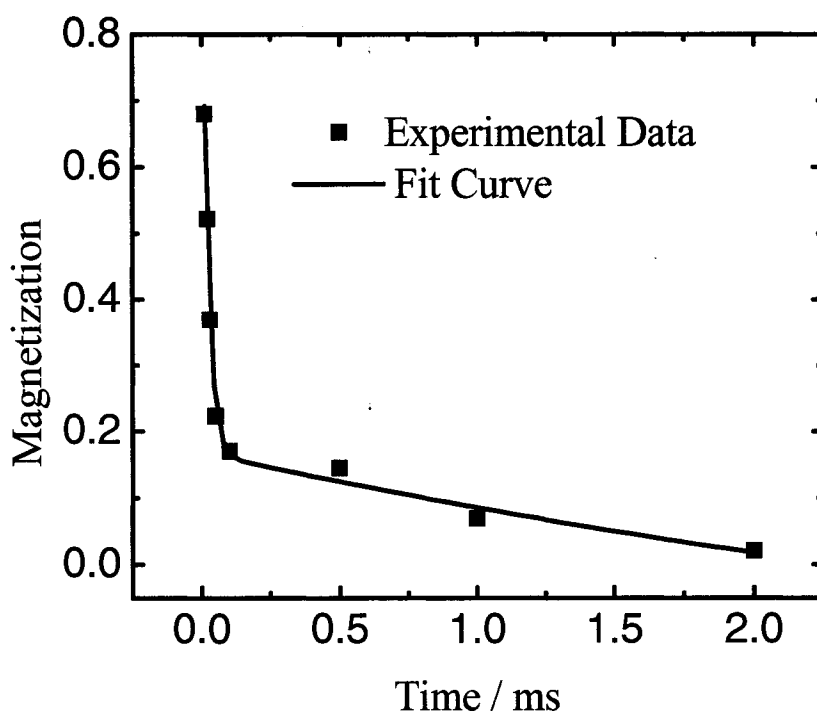
Figure 5.4 The ^{13}C T_2 relaxation for the non-crystalline peak of HPDE film 04-07885.

5.3.2 Summary on Phase Structure Determination

Similar to HDPE bulk samples, HDPE blown film 04-07885 is composed of four phases: the monoclinic crystalline, orthorhombic crystalline, amorphous, and crystalline-amorphous interfacial phases. The procedures discussed above can be applied to the other two HDPE films (04-08134 and 04-08135) without any modifications. Because it takes quite a long time to obtain the fully-relaxed spectra, the final phase structure determination of these two HPDE films was not been completely performed. The CP ^{13}C spectra of these two films were obtained, and are shown in Figure 5.5.

δ / ppm
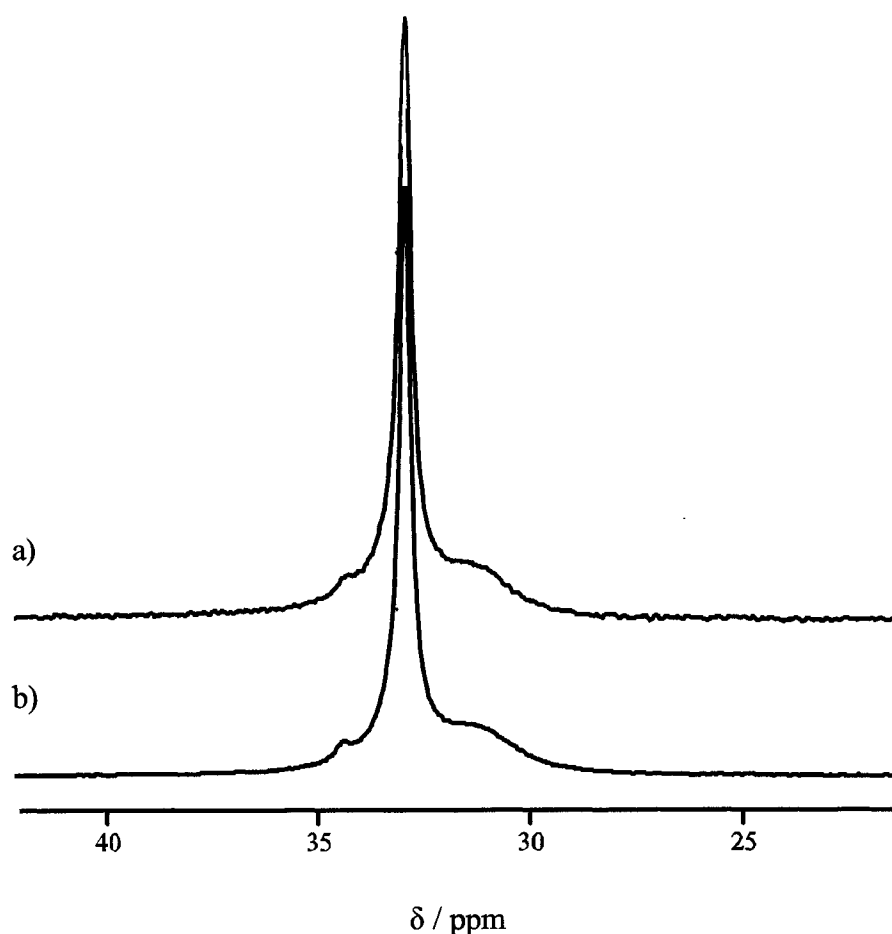
Figure 5.5 CP ^{13}C NMR spectra of HDPE films: a) 04-08134; b) 04-08135.

5.3.3 The Location of the Hexyl Branches

Figure 5.6 shows the ^{13}C NMR spectrum of ss-LLDPE-M2 obtained with the modified spin-echo pulse sequence with TTPM decoupling with τ =25 μs. The peak at 31.0 ppm is that for the non-crystalline components, and the one at 32.9 ppm is that for the crystalline component. Because the pulse delay was 5 s, which is much smaller than T_1 of the orthorhombic crystalline peak, this peak is suppressed due to saturation. The peak at 15.0 ppm is that for the CH_3 carbons, and the one near 25 ppm is for the CH_2 carbons which are adjacent to the CH_3 end groups. The peak at 38.0 ppm is the signal for the CH carbons at the branching site. The concentration of this type of carbon atoms is low, thus, giving rise to a small peak.

δ /ppm
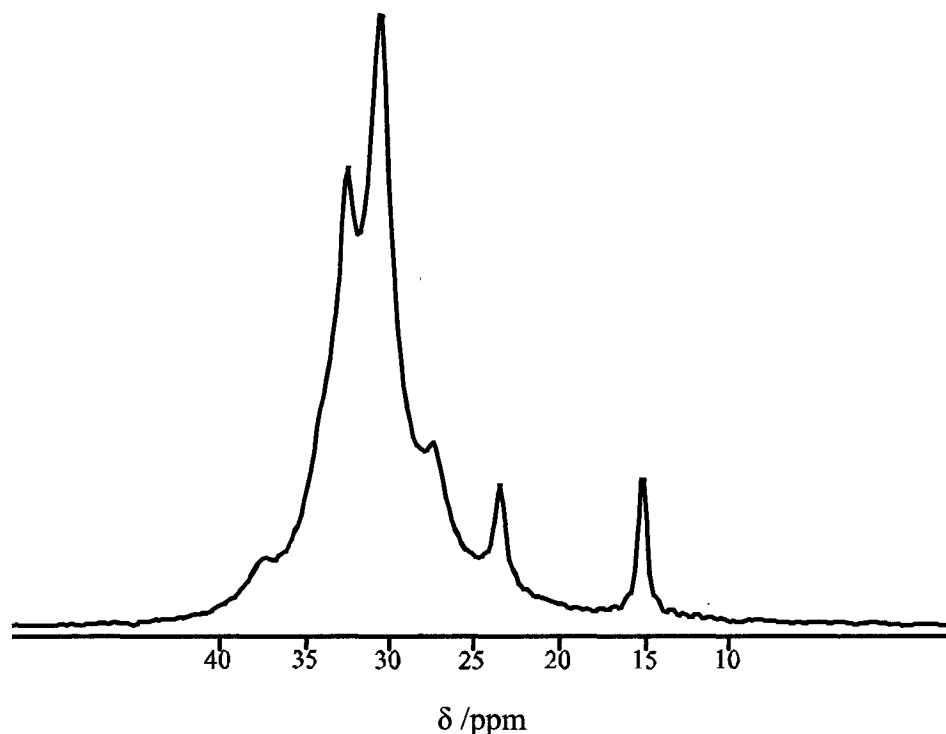
Figure 5.6 The ^{13}C NMR spectrum of ss-LLDPE-M2 obtained with the modified spin-echo pulse sequence at τ =25 μs.

- 56 -

T_2 measurements for the ^{13}C nuclei of both the CH_2 (the peak at 31.0 ppm) and CH carbons (the peak at 38.0 ppm) were performed. Figure 5.7 shows the T_2 relaxation process for the non-crystalline components (the peak at 31.0 ppm) of ss-LLDPE-M2. Two components with different T_2 values and the associated mass fractions were determined following the same procedures as discussed in Chapter 4. The results are summarized in Table 5.4.
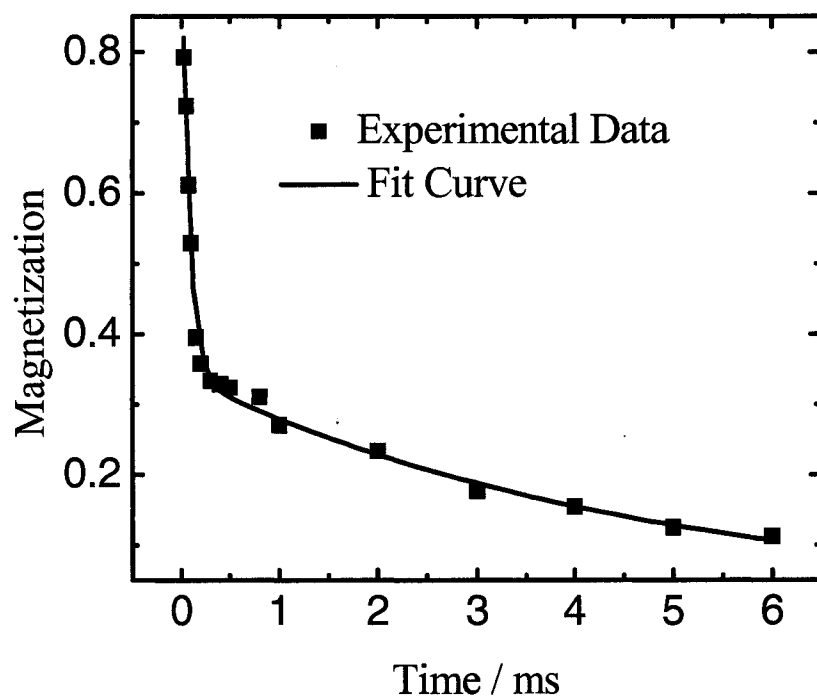
Figure 5.7 T_2 relaxation process for the non-crystalline components of ss-LLDPE-M2.

The T_2 relaxation behaviour for the CH carbons at the branching sites is shown in Figure 5.8. Likewise, two components with different T_2 values and their

- 57 -

associated mass fractions were determined. The existence of two components with different T_2 values implies that the short-chain branches reside at two different environments, namely, the interphase and amorphous phase. The results are summarized in Table 5.4.
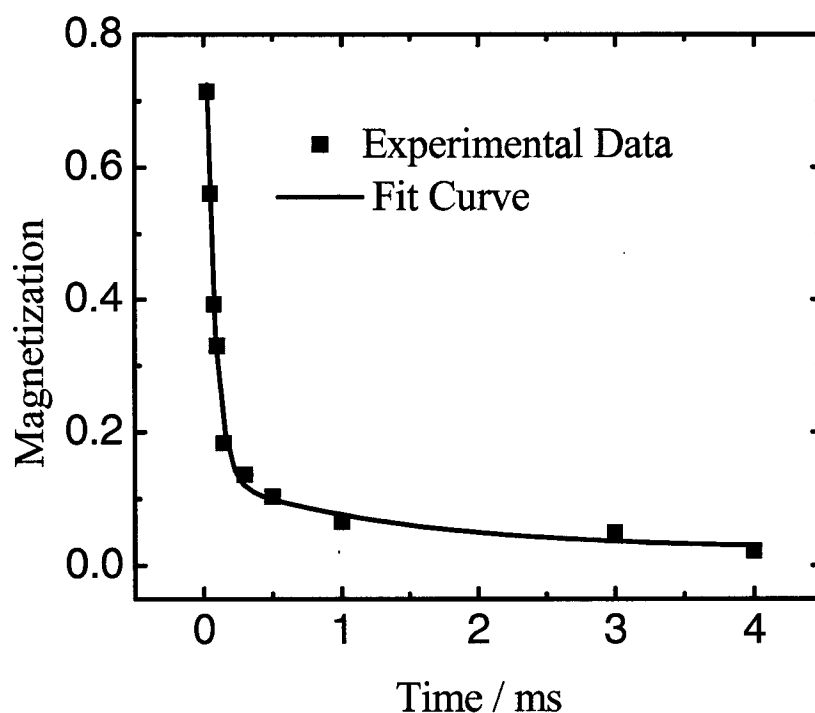
Figure 5.8 T_2 relaxation behaviour for the CH carbons at the branching sites of ss-LLDPE-M2.

The same procedures were also applied to ZN-LLDPE-A2, and the results obtained are also summarized in Table 5.4. The analyses indicate that the branches are not very evenly distributed between the interfacial and amorphous regions for both of ss-LLDPE-M2 and ZN-LLDPE-A2. It seems that ss-LLDPE-M2 has a

- 58 -

greater density of branches in the interfacial region than that in the amorphous region, while for ZN-LLDPE-A2, it is the amorphous region that contains the greater portion of branches. It is also observed that although the two LLDPE samples have similar branch contents, ss-LLDPE-M2 has a larger interfacial region than ZN-LLDPE-A2. This observation is comparable with the results obtained for LLDPEs with much lower average branch contents, as shown in Chapter 4.

Table 5.4 Summary of the partitioning results.

Sample		T_2 (ms)	Mass fraction (%)
ss-LLDPE-M2	Interfacial	0.08	66
	Amorphous	4.7	34
	Interfacial methine carbon	0.07	87
	Amorphous methine carbon	3.4	13
ZN-LLDPE-A2	Interfacial	0.1	46
	Amorphous	1.8	54
	Interfacial methine carbon	0.08	25
	Amorphous methine carbon	1.2	75

As discussed above, the signals for the CH carbons at the branching sites are rather weak, and considering the signal will decrease with increasing τ values, this combination of situations made the measurements very difficult and accordingly

- 59 -

significant errors may occur. Therefore, the above results may not be reliable. New

methods to accurately measure the signals are required to confirm these results.

5.4 References

Alamo, R.G. and Mandelkern, L. (1989) Thermodynamic and Structural Properties of Ethylene Copolymers, *Macromolecules* 22, 1273-1277.

Alamo, R.G.; Domszy, R. and Mandelkern, L. (1984) Thermodynamic and Structural Properties of Copolymers of Ethylene, *J. Phys. Chem.* 88, 6587-6595.

Horii, F.; Kaji, H.; Ishida, H.; Kuwabara, K.; Masuda, K. and Tai, T. (1998) Solid-State NMR Analyses of the Structure and Dynamics of Polymers in the Different States, *J. Mol. Struc.* 441, 303-311.

Kitamaru, R.; Horii, F. and Murayama, K. (1986) Phase Structure of Lamellar Crystalline Polyethylene by Solid-State High-Resolution ^{13}C NMR: Detection of the Crystalline-Amorphous Interphase, *Macromolecules* 19, 636-643.

Kuwabara, K.; Kaji, H.; Horii, F.; Bassett, D. C. and Olley, R. H. (1997) Solid-State ^{13}C NMR Analyses of the Crystalline-Noncrystalline Structure for Metallocene-Catalyzed Linear Low-Density Polyethylenes, *Macromolecules* 30, 7516-7521.

Mandelkern, L. (1990) The Structure of Crystalline Polymers, *Acc. Chem. Res.* 23, 380-386.

Perez, E.; VanderHart, D. L.; Crist Jr, B. and Howard, P. R. (1987) Morphological Partitioning of Ethyl Branches in Polyethylene by ^{13}C Nuclear Magnetic Resonance, *Macromolecules* 20 78-87.

Shimizu; Y.; Harashina, Y.; Sugiura, Y. and Matsuo, M. (1995) Morphology and Molecular Mobility of Several Kinds of Polyethylene Specimens by ^{13}C Solid-State NMR and X-ray Diffraction Techniques, *Macromolecules* 28, 6889-6901.

Torchia, D. A. (1978) The Measurement of Proton-Enhanced Carbon-13 T_1 Values by a Method Which Suppresses Artifacts, *J. Magn. Reson.* 30, 613-617.

VanderHart, D. L. and Perez, E. (1986) A ^{13}C NMR Method for Determining the Partitioning of End Groups and Side Branches between the Crystalline and Noncrystalline Regions in Polyethylene, *Macromolecules* 19, 1902-1909.

Young, R.J. and Lovell P.A. (1991) Introduction to Polymers (Second Edition), Nelson Thornes Ltd, UK.

CHAPTER 6

Tensile Testing

6.1 Introduction

Mechanical testing is another important aspect in structure-property correlations. Mechanical properties of polyethylene blown films have been widely investigated [Zhang *et al.* 2004; Lu *et al.* 2001; Krishnaswamy and Sukhadia 2000; Godshall *et al.* 2003]. Structural features, such as the degree of crystallinity, molecular weight and its distribution, concentration and distribution of branches, and size and orientation of the crystalline lamella, are among the key factors that control the mechanical performances [Zhang *et al.* 2004; Godshall *et al.* 2003]. Generally speaking, HDPE films show medium tensile properties, while LLDPE films have a wide range of tensile performances due to their varying short-chain branch contents [Zhang *et al.* 2004].

Tensile strengths of four selected polyethylene films were tested according to ASTM D 882-02 on an INSTRON 4202 machine. Details are discussed below.

6.2 Experimental Section

6.2.1 Materials

Four film samples, obtained from NOVA Chemicals Corp. in Calgary, Canada, were tested. The characteristics of the films are listed in Table 6.1.

- 62 -

Table 6.1 Characteristics of four film samples

Film	Density (g/cm^3)	M.I. [a] (dg/min)	M_n	M_w	M_z	PDI [b]	Branch Content [c]	Type of Comonomer
04-07885 [d]	0.9591	1.23	18,800	109,200	427,900	5.81	Nil	
04-10428 [e]	0.9174	0.73	28,000	100,400	236,500	3.59	17.0	Octene
04-16416 [e]	0.9165	0.97	31,900	97,600	231,200	3.06	16.2	Octene
04-17755 [e]	0.9130	0.88	27,500	108,300	356,400	3.94	19.7	Octene

[a] Melt Index
[b] Polydispersity index
[c] Per 1000 backbone carbons
[d] HDPE film
[e] ss-LLDPE film

6.2.2 Experimental Methods

The standard test method, used for tensile properties of thin plastic sheeting, is ASTM D 882-02. An INSTRON 4202 machine was used and the test method is Grab Test CGSB. The crosshead speed was set to 200 mm/min, and the initial grip separation was 25 mm for all tests. The films were cut into 60×10 mm rectangular geometry. Five specimens were used for the tensile strength tests for the machine direction (MD) and transverse direction (TD), respectively. Prior to the tests, the samples were placed in a room with 65% humidity for 24 h conditioning. The test conditions are summarized in Table 6.2.

Table 6.2 Test conditions for the films

Films	Initial grip separation (mm)	Crosshead speed (mm/min)	Temperature (°C)	Thickness (μm)
04-07885 (HDPE)	25	200	20	44
04-17755 (ss-LLDPE)	25	200	20	55
04-10428 (ss-LLDPE)	25	200	20	44
04-16416 (ss-LLDPE)	25	200	20	110

6.3 Results and Discussion

The tensile strength test curves for 04-10428 LLDPE film in the MD and TD directions are shown in Figures 6.1 (a) and (b), respectively. The results show that the fracture load in MD is higher than that in TD, whereas the fracture displacement is larger for TD than that for MD. Similar results were also observed for 04-17755 and 04-16416. Using HDPE film sample which has the highest density as the standard, 04-17755 and 04-10428 show poorer tensile performances in both MD and TD, while 04-16416 shows stronger tensile strength in both MD and TD. Table 6.3 summarizes the test results for the films. It is obvious that tensile strength of the polymer not only depends on the degree of crystallinity but also other structural features of the film. Otherwise, the HDPE film would have the highest tensile strength among the film samples. It is also clear from the data that ss-LLDPE film 04-10428 exhibited the largest difference in the TD and MD tensile properties. The physical origin of this observation is unclear yet.
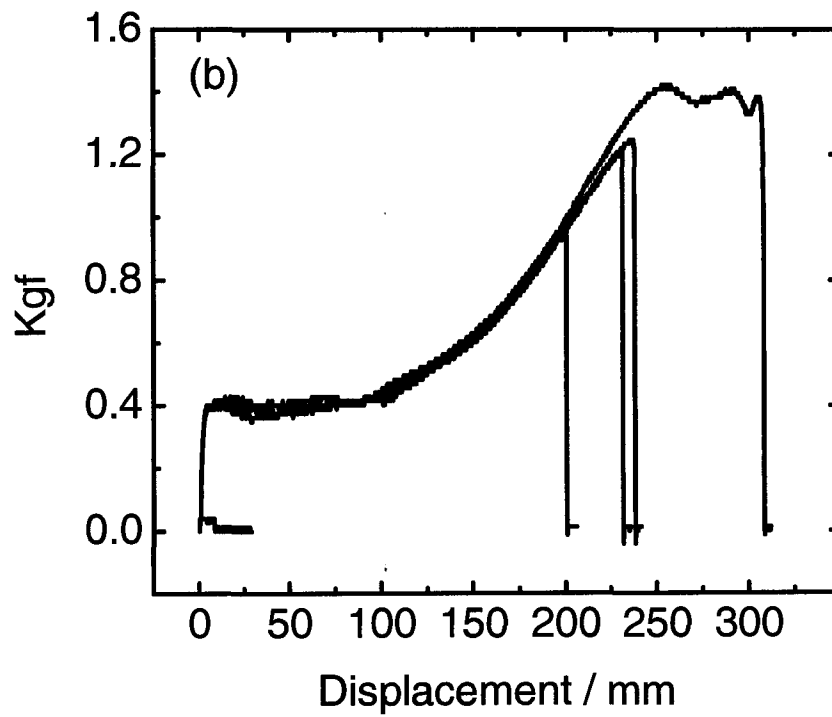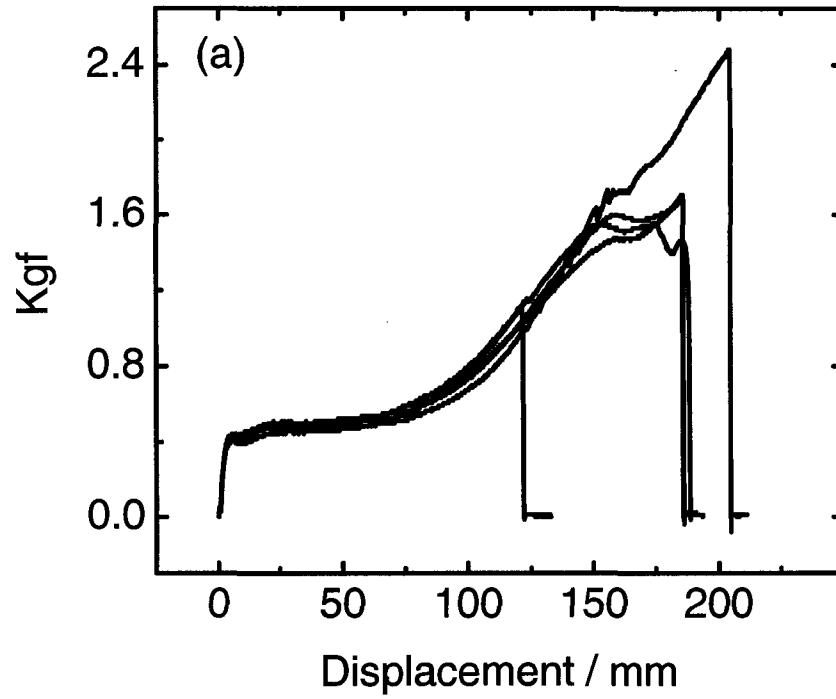
- 64 -

Figure 6.1 Tensile strength of film sample 04-10428: (a) MD; (b) TD.

Table 6.3 Summary of the tensile properties of four film samples

Sample	Tensile strength Break (kgf)	Displacement at Break (mm)
F07885	3.5256±0.3500	234.46±29.60
F17755 (MD)	1.7664±0.2793	231.36±67.44
F17755 (TD)	1.7478±0.3491	250.90±39.68
F10428 (MD)	1.7048±0.4982	174.58±31.57
F10428 (TD)	1.1648±0.1974	225.24±24.93
F16416 (MD)	4.5532±0.6854	260.74±18.58
F16416 (TD)	4.1286±0.9969	303.76±41.10

6.4 References

Godshall, D.; Wilkes, G.; Krishnaswamy, R. K. and Sukhadia, A. M. (2003) Processing-Structure-Property Investigation of Blown HDPE Films Containing Both Machine and Transverse Direction Oriented Lamellar Stacks, *Polymer* 44, 5397-5406.

Krisnaswamy, R. K. and Sukhadia, A. M. (2000) Orientation Characterization of LLDPE Blown Films and Their Implications on Elmendorf Tear Performance, *Polymer* 41, 9205-9217.

Lu, J.; Sue, H. J. and Rieker, T. P. (2001) Dual Crystalline Texture in HDPE Blown Films and Its Implication on Mechanical Properties, *Polymer* 42, 4635-4646.

Zhang, X. M.; Elkoun, S.; Ajji, A. and Huneault, M. A. (2004) Effect of Crystalline Structure on Tear Resistance of LDPE and LLDPE-Blown Films, *Journal of Plastic Film and Sheeting* 20, 43-52.

Zhang, X. M.; Elkoun, S.; Ajji, A. and Huneault, M. A. (2004) Oriented Structure and Anisotropy Properties of Polymer Blown Films: HDPE, LLDPE and LDPE, *Polymer* 45, 217-229.

CHAPTER 7

Conclusions and Future Work

7.1 Structure of Polyethylene

Solid-state ^{13}C NMR techniques are widely used to study structure and dynamics of polyethylenes [Kuwabara et al. 1997; Kitamaru et al. 1986; Matsumoto et al. 1996; Spiess 2004; Kaji and Horii 1997; Horii et al. 1998; Terao 1998; Earl and VanderHart 1979; Qiu and Mirau 2000; Schmidt-Rohr et al. 1992]. Fuming nitric acid (FNA) etching, followed by GPC measurements is a very useful method to study crystalline lamella size and its distribution of polyethylenes [Cook et al. 2000; Capaccio and Ward 1981; 1982]. This work attempts to investigate the morphological features of polyethylenes by the combination of these two methods. In particular, the morphological features of single-site (ss-) and Ziegler-Natta (ZN-) LLDPEs were probed.

The analyses of the ^{13}C spin-lattice (T_1) and spin-spin (T_2) relaxation times show that polyethylene samples consist of three components, which can be assigned to the crystalline, crystalline-amorphous interfacial, and amorphous phases, respectively. The degree of crystallinity was determined by measuring the relative intensities of the crystalline peak from the fully-relaxed ^{13}C NMR spectra. It was found that with comparable average branch content, the degree of crystallinity for ZN-LLDPE is higher than that for ss-LLDPE. The mass ratio for the interfacial component can be determined from the evaluation of the T_2 relaxation studies. The

results show that the mass fraction of the interphase for ZN-LLDPE is lower than that for ss-LLDPE.

FNA etching, followed by GPC and solid-state ^{13}C NMR analyses, was implemented to determine the lamella stem length and estimate the thickness of the interfacial region. It was found that ZN-LLDPE has thicker crystalline lamella and a smaller interfacial region than ss-LLDPE.

7.2 The Location of Short-Chain Branches

It is known that branches longer than two carbons do not enter into the crystalline region under equilibrium conditions [VanderHart and Perez 1986; Perez *et al.* 1987; Alamo *et al.* 1984; Alamo and Mandelkern 1989]. However, accurate partitioning of the branches between the interfacial and amorphous regions has not been resolved; yet, such information is important, because the location will affect the molecular mobility and free volume, and hence result in different mechanical properties. Kuwaba *et al.* [1997] have done some work on the clarification of the partitioning of the branches between the interfacial and amorphous regions. They found the branches are almost evenly distributed between the interfacial and amorphous regions. The clarification of the location of hexyl branches for ss-LLDPE-M2 and ZN-LLDPE-A2 has been performed based on their work.

The ^{13}C T_2 relaxation times of the methine carbons at the branching sites were measured by the modified spin-echo pulse sequence [Hirai *et al.* 1990] with TTPM decoupling [Bennett *et al.* 1995] only during the acquisition period. The mass ratio of the methine carbons in the interfacial and amorphous regions was

determined from the evaluation of the T_2 relaxation times. It was found that that the branches are not very evenly distributed between the interfacial and amorphous regions through the comparison of the mass ratios of the CH and CH_2 carbons in the interfacial and amorphous regions. For ss-LLDPE-M2, the interfacial region has a greater density of branches. For ZN-LLDPE-A2, the amorphous region has a greater density of branches.

7.3 Recommendations for Future Work

As discussed above, the combination of solid-state ^{13}C NMR techniques and FNA etching followed by GPC measurements is a powerful technique for the elucidation of morphological features of polyethylene samples. Therefore, this method can be further utilized to study polyethylene systems, such as ss-LLDPE films. Tensile strength tests of the available HDPE and ss-LLDPE films were carried out and the results have shown that the degree of crystallinity is not the only parameter that determines their tensile properties. Therefore, morphological features that account for the tensile properties of these ss-LLDPE films shall be determined. And finally, the correlation of the detailed morphological features with the mechanical performances also needs to be investigated.

Because the concentrations of the branches in the LLDPE samples we used are rather low (1-3%), and because a significant portion of the magnetization is lost due to the increased echo times, it usually takes 4K or even more transients to obtain sufficient signals from the CH carbons at the branching sites, making the experiments on a series of samples impractical. Also, the relative low quality of the

peaks brings uncertainty to the experimental results, which greatly affect the analysis. Future developments on better resolving the signals from CH carbons at the branching sites are needed.

Solid-state ^{13}C NMR techniques are very powerful for elucidating polyethylene structures and dynamics. This work mainly utilized the chemical shift and the relaxation behaviour to study the polyethylene system, and only in the 1D category. 2D and even higher-order NMR techniques may allow us to reveal more structural details about polyethylene systems. For example, wide-line separation 2D NMR spectra, developed by Spiess *et al.* [1992], are able to unravel important structural information about polymer systems. Therefore, 2D NMR techniques are strongly recommended for future studies.

7.4 References

Cook, J. T. E.; Klein, P. G.; Ward, I. M.; Brain, A. A.; Farrar, D. F. and Rose, J. (2000) The Morphology of Nascent and Moulded Ultra-High Molecular Weight Polyethylene. Insights from Solid-State NMR, Nitric Acid Etching, GPC and DSC, *Polymer* 41, 8615-8623.

Capacccio, G and Ward, I. M. (1981) Structural Studies of Ultrahigh-Modulus Linear Polyethylene Using Nitric Acid Etching and Gel Permeation Chromatography. I. Determination of the Crystal Size Distribution, *J. Polym. Sci.: Polym Phys. Ed.* 19, 667-675.

Capacccio, G and Ward, I. M. (1982) Structural Studies of Ultrahigh-Modulus Linear Polyethylene Using Nitric Acid Etching and Gel Permeation

Chromatography. II. Influence of Polymer Molecular Weight, Draw Temperature, and Annealing, *J. Polym. Sci.: Polym Phys. Ed.* 20 1107-1128.

Earl, W. L. and VanderHart, D. L. (1979) Observations in Solid Polyethylenes by Carbon-13 Nuclear Magnetic Resonance with Magic Angle Sample Spining, *Macromolecules* 12, 762-767.

Kuwabara, K.; Kaji, H.; Horii, F.; Bassett, D. C. and Olley, R. H. (1997) Solid-State ^{13}C NMR Analysis of the Crystalline-Noncrystalline Structrue for Metallocene-Catalyzed Linear Low-Density Polyethylene, *Macromolecules* 30, 7516-7521.

Kitamaru, R.; Horii, F. and Murayama, K. (1986) Phase Structure of Lamellar Crystalline Polyethylene by Solid-State High-Resolution ^{13}C NMR: Detection of the Crystalline-Amorphous Interphase, *Macromolecules* 19, 633-643.

Perez, E.; VanderHart, D. L.; Crist Jr, B. and Howard, P. R. (1987) Morphological Partitioning of Ethyl Branches in Polyethylene by ^{13}C Nuclear Magnetic Resonance, *Macromolecules* 20, 78-87.

Qiu, X. and Mirau, P. A. (2000) WIM/WISE NMR Studies of Chain Dynamics in Solid Polymers and Blends, *J. Magn. Reson.* 142, 183-189.

Schmidt-Rohr, K.; Clauss, J. and Spiess, H. W. (1992) Correlation of Structure, Mobility, and Morphological Information in Heterogeneous Polymer Materials by Two-Dimensional Wideline-Separation NMR Spectroscopy, *Macromolecules* 25, 3273-3277.

Spiess, H. W. (2004) Advanced Solid-State Nuclear Magnetic Resonance for Polymer Science, *J. Polym. Sci.: Part A: Polym. Chem.* 42, 5031-5044.

VanderHart, D. L. and Perez, E. (1986) A ^{13}C NMR Method for Determining the Partitioning of End Groups and Side Branches between the Crystalline and Noncrystalline Regions in Polyethylene, *Macromolecules* 19, 1902-1909.